Recombinant Adiponectin Peptide Ameliorates Cortical Neuron Damage Induced by Chronic Cerebral Hypoperfusion by Inhibiting NF-κB Signaling and Regulating Microglial Polarization

li'an Huang (huanglian1306@126.com)
Jinan University First Affiliated Hospital https://orcid.org/0000-0002-0416-7532
Wenxian Li
Xi'an Jiaotong University
Di Wei
The Fourth Military Medical University
Zheng Zhu
University of California Davis
Shuqin Zhan
Xi'an Jiaotong University
Ru Zhang
Xi'an Jiaotong University
Huqing Wang
Xi'an Jiaotong University
Guilian Zhang
Xi'an Jiaotong University

Research

Keywords: Chronic cerebral hypoperfusion, Adiponectin, microglial polarization, neuron damage, NF-κB

Posted Date: January 1st, 2021

DOI: https://doi.org/10.21203/rs.3.rs-137422/v1

Recombinant adiponectin peptide ameliorates cortical neuron damage induced by chronic cerebral hypoperfusion by inhibiting NF-κB signaling and regulating microglial polarization

Wenxian Li[1¶], Di Wei[2¶], Zheng Zhu[3¶], Shuqin Zhan[1], Ru Zhang[1], Huqing Wang[1], Guilian Zhang[1*], Li'an Huang[4*]

[1] Department of Neurology, The Second Affiliated Hospital, Xi'an jiaotong University, Xi'an, Shanxi, China.

[2] Department of Urology, Xijing Hospital, The Fourth Military Medical University, Xi'an, Shanxi, China.

[3] Department of Internal Medicine, Division of Hematology/Oncology, University of California Davis, Sacramento, CA 95817, USA.

[4] Department of Neurology, The First Affiliated Hospital, Jinan University, Guangzhou, Guangdong, China.

¶ These authors contributed equally to this study.

* Correspondence:

Prof. Guilian Zhang and Li'an Huang

zhgl_2006@126.com

Department of Neurology, The Second Affiliated Hospital, Xi'an Jiaotong University, XiWu Avenue, Xin Cheng District, Xi'an, Shaanxi, 710004, China

huanglian1306@126.com

Department of Neurology, The First Affiliated Hospital, Jinan University, 613 HuangPu Avenue West, Tian He District, Guangzhou, Guangdong, 510632, China

Abstract

Background

Chronic cerebral hypoperfusion (CCH) is common in multiple central nervous system diseases that are associated with neuronal death and cognitive impairment. Microglial activation-mediated polarization changes may be involved in CCH-induced neuronal damage. Adiponectin (APN) is a fat-derived plasma protein that affects neuroprotection. This study investigated whether a recombinant APN peptide (APN-P) improved the cognitive function of CCH rats by regulating microglial polarization in the cortex.

Methods

A CCH rat model was established through bilateral common carotid artery occlusion (BCCAO) surgery. An antibody microarray was used to analyze differentially expressed proteins in the cerebral cortex of CCH rats compared to the sham rats. APN-P and a solvent control were used to intervene at different time points. Western blotting and immunofluorescence staining were conducted to examine the status of microglial polarization in different treatment groups. qRT-PCR was used to detect the expression levels of inflammatory and anti-inflammatory genes. Neuronal morphology was assessed via Nissl staining, and cognitive function was assessed with the Morris water maze test. *In vitro*, by inhibiting the expression of NF-κB in BV2 microglia and using Transwell co-culture systems of BV2 microglia and neurons, the effects of APN-P on neuroprotection and the underlying mechanism were investigated.

Results

In the cortical microglia of 12-week-old CCH rats, the expression of APN protein was significantly downregulated compared to the sham rats. CCH damages neurons and activates cortical microglial polarization to an M1-type by upregulating inflammatory factors. APN-P supplementation upregulated APN expression in cortical microglia, with neuronal survival as well as microglial polarization from an M1 toward an M2 phenotype in CCH cortex. *In vivo* and *in vitro* experiments revealed that APN-P promoted the expression of anti-inflammatory factors and neuronal survival by inhibiting NF-κB signaling, thus improving the cognitive function in CCH rats.

Conclusions

Our study revealed a novel mechanism by which APN-P suppresses the NF-κB pathway and promotes microglial polarization from M1 toward the M2-type to reduce neuron damage in the cortex after CCH.

Keywords: Chronic cerebral hypoperfusion; Adiponectin; microglial polarization; neuron damage; NF-κB

Background

While the pathophysiology and mechanisms of acute stroke are of scientific and clinical importance, few experimental systems can recapitulate the ischemic injury that results from chronic cerebral hypoperfusion (CCH) [1]. CCH is a state of chronic cerebral blood flow (CBF) reduction that contributes to numerous neurological illnesses [2], and can result from disorders affecting the cerebral vascular system [3]. The long-lasting reduction in CBF will lead to neuronal damage

followed by cognitive and memory deficits [2]. Cognitive injury secondary to CCH is pervasive and likely underrecognized [1, 4]. To date, there is no successful drug treatment that prevents CCH-induced cognitive deficits [5, 6]. Although improving cerebral perfusion can be an effective intervention, it is limited to only early stages of CCH.

In response to CCH, a chain of homeostatic interactions occur in the brain, including neuroinflammation, oxidative stress, mitochondrial dysfunction, disorder of neurotransmitter system and lipid metabolism, and changes in expression of growth factors, which culminate in neuronal death [4, 7]. Unfortunately, the neurorestorative potential of the adult brain is very limited [8]. Previous studies have reported that neuronal death is the key factor for cognitive impairment in CCH [7, 9, 10], with CCH patients often suffering long-term neurological deficits and cognitive impairment in the process of cerebral hypoperfusion [2]. Indeed, a previous study indicated that patients with vascular cognitive impairment exhibited typical neuron loss [11]. Identifying promising strategies for reducing neuronal death is paramount for long-term functional improvement in CCH patients.

CCH does not influence acute neural cell death but can induce a chronic phase of neuronal degeneration, death, and loss. Chronic cerebral ischemia and neural death are accompanied by long-lasting neuroinflammation. Chronic neuroinflammation is tightly related to neuronal death [5], suggesting that reducing neuronal death could be a promising therapeutic opportunity for improving the neurological outcomes of CCH.

Microglia are innate immune cells of the central nervous system and are the major mediators of neuroinflammation, microglia can be activated to polarize after stimulation, which exerts pro-inflammatory or anti-inflammatory functions through the secretion different substances [12] .

Neuroinflammation has been linked strongly to cognitive deficits, activated (proinflammatory) microglia can reduce new cell survival and may also affect their integration into pre-existing neural networks [13]. Activated microglia can have M1 and M2 phenotypes: M1 microglia are pro-inflammatory and secrete inflammatory cytokines that promote neuronal damage under pathological conditions, while M2 microglia express anti-inflammatory mediators that prevent inflammation and contribute to neurological protection [14].

In our previous study, we reported that the CCH process can lead to activation of microglia in the brain [7]. Indeed, mounting evidence has demonstrated that the microglia with the anti-inflammatory phenotype play a neurorestorative role during the recovery period after ischemic events [8]. However, the process of cerebral microglial polarization in CCH is not clear. Hippocampal microglial polarization was shown to be associated with the M1 phenotype during CCH [12], and therefore, regulating the polarization of microglia in the brain may be a novel therapeutic target for neurological recovery after CCH.

Adiponectin (APN) is mainly secreted by mature adipocytes and can function as an insulin-sensitizing adipokine, with a globular domain that acts as its functional region [15]. APN is the main adipokine controlling the balance of energy metabolism at both cellular and systemic levels [16], and APN is considered a biomarker for metabolic diseases in multiple systemic systems because it has significant antiatherosclerotic, antiapoptotic, organ-protective, anti-inflammatory, and other biological functions [15]. APN and its receptor are expressed in the central nervous system of mammals; additionally, peripheral APN can enter the cerebrospinal fluid through blood circulation [17]. Recent studies [13, 17-19] have shown that APN is closely associated with neurological diseases and that APN has neuroprotective effects. A clinical study has shown that APN levels <4 μg/mL is independently

associated with mortality, and low plasma APN is related to an increased risk of 5-year mortality after first-ever ischemic stroke [20]. The reduction of APN levels can weaken anti-inflammatory capacity and increase susceptibility to the ischemic vascular disease progression [17, 18]. In the serum of elderly patients with type 2 diabetes, APN levels are decreased, and this is closely related to the outcome of neurocognitive impairment [19]. Moreover, as a biomarker that represent one of the inflammation, APN can be used as a marker in patients with clinical cognitive impairment [13]; however, the exhaustive effects of APN on and neuroinflammation microglial polarization following CCH are not well elucidated. Furthermore, due to the limited blood-brain barrier penetrability of the full length APN, adenovirus-mediated and intracerebroventricular injection for APN supplementation may be traumatic and unsuitable for clinical practice. According to the amino acid sequence of the functional globular domain at the C-terminal end of APN, a variant APN peptide (APN-P) that can effectively cross the blood-brain barrier was used in this study [16, 21].

Antibody microarray experiments are used as the initial tool during the biomarker discovery process [22]. In this study, using antibody microarray, we showed that the APN protein levels decreased in the cortex 12 weeks after CCH. A better understanding of the interactions between microglial polarization and APN might provide new therapeutic targets for the treatment of CCH. To address this challenge, we attempted to explore the role and underlying mechanisms of two subtypes of activated microglia-mediated neuroinflammation, as well as the interactions between microglial polarization and neuronal death in CCH, with or without APN-P treatment.

Materials and Methods

Animals and Ethics

A total of 138 eight-week-old healthy, adult male Sprague-Dawley rats weighing 200–250 g were obtained from the Laboratory Animal Center of Fourth Military Medical University. All rats were housed in a specific pathogen-free animal room at a constant temperature (23°C ± 1°C) and humidity (60% ± 10%) in a 12-h light/dark cycle. The rats were conditioned for 4 weeks before the experiments started and given free access to food and water. All animal experimental procedures were approved by the Ethics Committee for Animal Experimentation of the Xi'an Jiaotong University, and followed the National Institutes of Health Guide for the Care and Use of Laboratory Animals [12].

Animal surgery

Rats were anesthetized with 3% sodium pentobarbital [50 mg/kg, intraperitoneal (i.p.) injection]. Rats were subjected to permanent bilateral common carotid artery occlusion (BCCAO) surgery to induce CCH as described previously [2, 7, 12]. Briefly, both common carotid arteries were ligated with two 4-0 sutures. Sham rats underwent bilateral common carotid artery exposure but not artery occlusion.

Cell cultures

The mouse microglia cell line BV2 and mouse hippocampal neuronal cell line HT-22 were purchased from the China Center for Type Culture Collection. BV2 and HT-22 cells were cultured in high-glucose Dulbecco's modified Eagle medium (DMEM, Hyclone, USA), supplemented with 10% fetal bovine serum (Gibco, USA) and 1% penicillin-streptomycin solution (Gibco, USA). Cells were incubated in 5% CO_2 humidified atmosphere at 37°C. BV2 and HT-22 cells were seeded into

6-well plates at a density of 2×10^5 cells/mL. Primary neuronal cultures were harvested from the cerebral cortices of E16–E18 mouse embryos. Poly-D-lysine-coated culture plates or glass cover slips were prepared, then dissociated cells were obtained and seeded. The neurobasal medium (Gibco, USA) contained 2% B27 (Invitrogen, USA) and 1% penicillin and streptomycin. Primary cortical neurons were seeded in 6-well plates at a density of 4×10^5 cells/mL.

Drug administration

The synthetic peptide amino acid sequence of the recombinant APN-P is NH_2-LQVYGDGDHNGLYADNVN-COOH [23] **(Fig. 2a)**. For *in vivo* experiments, APN-P was dissolved in a 0.9% saline solution and administered to rats in the treatment group through every other day tail vein injections of 1 mg/kg APN-P immediately after BCCAO induction.

For *in vitro* experiments, we used 200 ng/mL lipopolysaccharide (LPS) (Sigma, USA) for 24 h to identify inflammatory responses in BV2 cells. APN-P was added to the medium 2 h before the addition of LPS. APN-P solutions at concentrations of 25 μM, 50 μM, and 100 μM were prepared, and 50 μM was selected for further experiments.

Experimental Design

Experiment 1. Differential expression analysis of cortical proteins in CCH rats using antibody microarrays. Fresh frozen cortex tissue was analyzed using antibody-based protein microarrays (sham group: n = 6; CCH 12w group: n = 6). A commercially available microarray (Biotin label-based rat antibody array, AAR-BLG-1, RayBiotech®, United States) was used, which included 90 antibodies made up of 16 classifications that included cytokines, neurokines, and chemokines, as

well as another 12 control antibodies. A detailed manufacturer's protocol was described in previous reports [7, 24].

Experiment 2: Neuroprotective effects of APN-P on microglial polarization induced by CCH and exploration of the underlying mechanisms *in vivo*. In total, 138 rats (27 rats in the sham group; 111 out of an initial 121 rats survived CCH surgery) were randomly and evenly divided into the sham, CCH [CCH 4 weeks (w) (4w after BCCAO surgery), CCH 8w, CCH 12w], and CCH+APN-P (CCH 4w+APN-P, CCH 8w+APN-P, CCH 12w+APN-P) treatment groups (1 mg/kg/Qod). After the CCH or intervention with APN-P, rats were tested for behavioral function using a water maze test, and were then sacrificed to evaluate immunofluorescence staining, neuronal morphology, western blotting and quantitative real-time PCR (qRT-PCR) analyses. Animal groups and the number of rats used in the study are shown in **Additional file 1**. Rats were euthanized by sodium pentobarbital overdose [100 mg/kg, intraperitoneal (i.p.) injection] at the corresponding experimental end points.

Experiment 3: Exploration of the mechanism of the protective role of APN-P *in vitro*. BV2 cells were cultured in a different type of dishes to approximately 80% confluence before intervention. The groups and interventions included: (1) control group: with conventional medium; (2) APN-P group: addition of 50 μM APN-P for 26 h in total; (3) LPS group: addition of 200 ng/mL LPS for 24 h in total; (4) LPS+BAY 11-7082 (BAY) group: we treated the cells with a known potent inhibitor of NF-κB, BAY (10 μM) for 30 min prior to stimulating the BV2 cells with LPS, then plus 200 ng/mL LPS for another 24 h; and (5) LPS+APN-P group: addition of 50 μM APN-P for 2 h prior to

stimulating the BV2 cells with LPS, then plus 200 ng/mL LPS for another 24 h.

Morris water maze test

Learning and spatial memory in the rats from different groups were evaluated with the Morris water maze test 4, 8, and 12 weeks after BCCAO using a previously described method [7]. The mean escape latency (EL) of four training sessions was recorded as a daily learning score from the 1st to 5th day. The swimming path and number of times that the rats crossed the platform in 60 s on the 6th day were recorded as the score for spatial memory by the animal behavioral recording system.

Microglia-neuron co-cultures

HT-22 cells were plated into 24-well plates (2×10^4 cells/mL). BV2 cells were divided into the five groups as above in 0.4-μm pore-sized Transwell inserts (Costar, USA) (1×10^4 cells/mL)). Thereafter, Transwell inserts and the medium from each group of BV2 cells was respectively collected and transferred to HT-22 cells for another 48 h. The HT22 cell viability was measured by the intensity of 5-chloromethylfluorescein diacetate (CMFDA) fluorescence to determine the effects of the secreted cytokines from each groups of BV2 cells.

For the indirect microglia-neuron co-cultures, primary cortical neurons were plated into 24-well plates (8×10^4 cells/mL) and incubated for 3 d. BV2 microglia were then added to 0.4-μm pore-sized Transwell inserts (Costar, USA) (1×10^4 cells/mL). After treatment, Transwell inserts and the medium from each group of BV2 cells was respectively collected and transferred, and the neurons and BV2 microglia were co-cultured for another 3 d. The viability of primary cortical neurons were measured via CCK-8 test.

Nissl staining

Nissl staining was used to observe morphological changes in neurons within the cortex of CCH rats. Rats were transcardially perfused (chest ribs were dissected to expose heart tissue for perfusion) with physiological saline solution followed by 4% paraformaldehyde [25] and following the manufacturer's instruction of the Nissl staining kit (E607316, Sangon Biotech, China). Neurons in three different fields were counted. Intact neurons were shown as a rich cytoplasm, one or two large round nuclei with large cell bodies, but damaged neurons were shown as dark cytoplasm, condensed nuclei, empty vesicles or shrunken cell bodies.

Immunofluorescence staining

***In vivo* experiments.** The selected brain slices were incubated with phosphate-buffered saline (PBS) solution with 0.1% Triton X-100 for 30 min, then blocked with PBS containing 5% goat serum (Gibco, USA) for another 30 min. The samples were incubated overnight at 4°C with the following primary antibodies: anti-Iba-1 (1:200; Abcam), anti-APN (1:200; Abcam), anti-CD16 (1:200; Abcam), anti-CD206 (1:200; Abcam), anti-NeuN (1:200; Abcam). The sections were rinsed in PBS and incubated with the corresponding secondary antibodies (Abcam) for 1 h at 25°C. Lastly, sections were incubated in 4,6-diamidino-2-phenylindole (DAPI) solution (Invitrogen, USA) for 15 min at 25°C. All section images were blindly captured using a fluorescence microscope (Nikon, Japan) and analyzed with the Image J software.

***In vitro* experiments.** BV2 cells were fixed with 4% formaldehyde solution, incubated with 0.1% Triton X-100 in PBS for 30 min, then blocked with 5% goat serum (Gibco, USA) in PBS for another

30 min. The samples were incubated overnight at 4°C with the following primary antibodies: anti-Iba-1 (1:200, Abcam), anti-CD16 (1:200, Abcam), anti-CD206 (1:200, Abcam). The appropriate secondary antibodies (Abcam) were used, and the nuclei were stained with DAPI (Invitrogen, USA). Sample images were captured with a fluorescence microscope (Nikon, Japan) and analyzed with the Image J software.

Western blotting

The selected samples were collected and homogenized in ice-cold RIPA buffer with 1% protease and phosphatase inhibitors, with an ultrasonic homogenizer. The lysates were centrifuged, then the supernatants were transferred to new frozen storage tubes (stored at -80°C). Protein concentrations were measured with a BCA Protein Assay kit (Thermo Fisher Scientific, USA). Protein samples were separated with SDS-PAGE, with 20 μg protein loaded into each well of the electrophoresis gels. The proteins were then transferred to PVDF membranes (Millipore, USA). Membranes were blocked with 5% non-fat milk in TBST and then incubated with primary antibodies overnight at 4°C, then each membranes were incubated with the appropriate secondary antibodies (1:5000, Abcam) at room temperature for another 2 h. After washing three times for 5 min in TBST, the protein bands were detected using a Bio-Rad Imaging System (Bio-Rad, USA). The following primary antibodies were used: anti-APN (1:800, Abcam); anti-iNOS (1:1000, Abcam); anti-Arginase-1 (Arg-1) (1:1000, Abcam); anti-NF-κB (P65, 1:800, Cell Signaling Technology); anti-phospho-NF-κB (p-P65, 1:800, Cell Signaling Technology); anti-β-actin (1:3000, Abcam).

qRT-PCR

Cortex tissue of rats and BV2 cells were collected from each treatment groups. Total RNA was isolated using an RNA Extraction Kit (Thermo Fisher Scientific, USA) and quantified. Then, reverse transcription using a reverse transcriptase kit (TaKaRa, Japan). Real-time PCR was performed according to the manufacturer's manual for SYBR green (TaKaRa, Japan). The reaction was performed at 95°C for 3 min followed by 40 cycles of 95°C for 10 s and 55°C for 30 s on the Bio-Rad PCR Detection System (Bio-Rad, USA). The primers (**Table 1**) and sequences derived from the relative mRNA expression levels were calculated using the $2^{-\Delta\Delta CT}$ method and the data were presented normalized by β-actin.

Table 1 Primers used for qRT-PCR

Primers	Species	Forward (5'-3')	Reverse (5'-3')
iNOS	Rat	TTCACGACACCCTTCACCACA	TCTCTGGGTCCTCTGGTCAAAC
	Mice	CAACAGGAACCTACCAGCTCACT	AGCCTGAAGTCATGTTTGCCG
IL-6	Rat	AAGAGACTTCCAGCCAGTTGCC	TGTGGGTGGTATCCTCTGTGAAG
	Mice	TTCTTGGGACTGATGCTGGTG	GCCATTGCACAACTCTTTTCTC
IL-18	Rat	GGAATCAGACCACTTTGGCAGA	GTCTGGTCTGGGATTCGTTGG
	Mice	TGAAGTAAGAGGACTGGCTGTGA	TTGGCAAGCAAGAAAGTGTCC
IL-1β	Rat	AATGGACAGAACATAAGCCAACA	CTTCTTCTTTGGGTATTGTTTGG
	Mice	TGCCACCTTTTGACAGTGATG	TGATGTGCTGCTGCGAGATT
TNF-α	Rat	CCAGGTTCTCTTCAAGGGACAA	GGTATGAAATGGCAAATCGGCT
	Mice	CCCTCACACTCACAAACCACC	CTTTGAGATCCATGCCGTTG
Arg-1	Rat	CACCTGAGTTTTGATGTTGATGG	CTCTGGCTTATGATTACCTTCCC
	Mice	GGTGGCAGAGGTCCAGAAGAA	CCCATGCAGATTCCCAGAGC
IL-10	Rat	GCACTGCTATGTTGCCTGCTC	CCCAAGTAACCCTTAAAGTCCTG
	Mice	TTTAAGGGTTACTTGGGTTGCC	AATGCTCCTTGATTTCTGGGC
TGF-β	Rat	CCAACTACTGCTTCAGCTCCACA	GCTTGCGACCCACGTAGTAGA
	Mice	CAACAATTCCTGGCGTTACCT	GCCCTGTATTCCGTCTCCTT
β-actin	Rat	TGCTATGTTGCCCTAGACTTCG	GTTGGCATAGAGGTCTTTACGG
	Mice	GTGACGTTGACATCCGTAAAGA	GTAACAGTCCGCCTAGAAGCAC

Cell viability assay

Cell Counting Kit-8 (CCK-8) (Dojindo, Japan) was used to assess primary neuron viability. The protocol was performed according to the manufacturer's manual. Briefly, in each 96-well plate, 10 μL CCK-8 solution was added to 90 μL medium solution and incubated for 4 h at 37°C. The absorbance at 450 nm was measured with a microplate reader (Thermo Fisher Scientific, USA).

CMFDA labeling

HT-22 cells were labeled with CMFDA (1 μM; C2925; Invitrogen) before initiating the co-culture with BV2 cells in different treatment groups. The experimental steps were performed according to the manufacturer's manual. Briefly, HT22 cells were cultured in a medium containing 1 μM CMFDA for 30 min then co-cultured with BV2 cells.

Statistical analyses

Data sets were analyzed using SPSS version 19.0 software (SPSS Inc., Chicago, IL). All values are expressed as the mean ± SD and are indicated in the figure legends. The statistical analysis was performed by comparing the means of two groups using an unpaired two-tailed Student's t-test. For multiple comparisons, the data were analyzed by One-way ANOVA with Tukey's multiple comparison test. Assessment of MWM results were analyzed by Two-way ANOVA with Bonferroni *post hoc* test. Statistical significance was considered at $p < 0.05$.

Results

CCH induces microglial activation and decreases expression of APN in the rat cortex

In order to investigate how CCH affects the activation of microglia in the cortex, we generated a rat

299 model for CCH using BCCAO surgery. First, we evaluated the polarization of microglia in rats at 2,
300 4, 8 and 12 weeks after BCCAO surgery. Immunofluorescence staining showed that the number
301 cells in the cortex region that were positive for the microglial marker Iba-1 (Iba-1+ cells)
302 significantly increased at 4 weeks and gradually increased at 8 and 12 weeks after BCCAO surgery
303 [sham vs. CCH 2w ($F = 0.43$, $P > 0.05$); sham vs. CCH 4w ($F = 0.00$, $P < 0.01$); sham vs. CCH
304 8w ($F = 1.93$, $P < 0.01$); sham vs. CCH 12w ($F = 4.50$, $P < 0.01$)]. Moreover, visualization of
305 the microglial morphologies indicated that CCH promoted microglia activation and
306 neuroinflammation (**Fig. 1b–c**). Spearman correlation analysis showed a negative correlation
307 between the number of Iba-1+ and NeuN+ cells [CCH 2w (correlation coefficient = -0.977, P =
308 0.023); CCH 4w (correlation coefficient = -0.961, P = 0.039); CCH 8w (correlation coefficient = -
309 0.962, P = 0.038); CCH 12w (correlation coefficient = -0.964, P = 0.036)] (**Fig. 1d**). Therefore,
310 CCH induced microglial activation, which was accompanied by neuronal damage in the cortex.
311 The protein arrays revealed that there were 10 differentially expressed proteins and APN expression
312 significantly decreased in cortex of the CCH rats (CCH 12w) compared to the sham rats (Fold
313 change: -4.23; $P < 0.05$) (**Fig. 1e**).
314 Double immunofluorescence staining showed that the percentage of APN-positive microglial
315 (APN+ Iba-1+)-cells in the cortex significantly decreased in the 12^{th} week after CCH compared to
316 the sham (27.11%±1.89 vs. 80.83%±5.59, $F = 10.36$, $P < 0.01$) (**Fig. 1f–g**).
317
318 **CCH polarizes microglia toward the M1 phenotype, while APN-P promotes the M2 phenotype**
319 In this study, as revealed by Western blotting, we found that APN expression was downregulated in
320 the cortex of CCH rats, especially CCH 12w, compared to the sham condition; however, after the

administration of APN-P (**Fig. 2b)**, APN expression was upregulated [(F = 236.27, CCH 4w vs. sham, P < 0.01; CCH 4w vs. CCH 4w +APN-P, P < 0.01), (F = 196.42, CCH 8w vs. sham, P < 0.01; CCH 8w vs. CCH 8w +APN-P, P < 0.01), (F = 271.02, CCH 12w vs. sham, P < 0.01; CCH 12w vs. CCH 12w +APN-P, P < 0.01)] (**Fig. 2b–c**). In addition, CCH increased the relative intensity (relative level) of iNOS (M1 marker), while APN-P treatment decreased the protein expression of iNOS [(F = 398.00, CCH 4w vs. sham, P < 0.01; CCH 4w vs. CCH 4w +APN-P, P < 0.01), (F = 415.82, CCH 8w vs. sham, P < 0.01; CCH 8w vs. CCH 8w +APN-P, P < 0.01), (F = 702.77, CCH 12w vs. sham, P < 0.01; CCH 12w vs. CCH 12w +APN-P, P < 0.01)]. While CCH decreased in the expression of Arg-1 (M2 marker), this expression was rescued by APN-P treatment in the CCH treatment group [(F = 22.30, CCH 4w vs. sham, P < 0.01; CCH 4w vs. CCH 4w +APN-P, P < 0.01), (F = 223.22, CCH 8w vs. sham, P < 0.01; CCH 8w vs. CCH 8w +APN-P, P < 0.01), (F = 204.98, CCH 12w vs. sham, P < 0.01; CCH 12w vs. CCH 12w +APN-P, P < 0.01)] (**Fig. 2b–c**).

Using double-immunofluorescence staining, the co-localization of the M1-associated marker CD16 or the M2-associated marker CD206 with Iba-1 was quantified (**Fig. 2d–e**). To clarify the characteristic activated microglia phenotype, the numbers of CD16-positive (CD16+) and CD206-positive (CD206+) microglia cells were analyzed, respectively. Compared to the sham group, the number of positive Iba-1+ cells and both microglia phenotypes gradually increased in the cortex of CCH rats from the 4^{th} to 12^{th} week, especially the number of CD16+ microglia (**Fig. 2d–h**). Compared to the CCH rats, APN-P treatment relieved microglia activation (neuroinflammation) according to the number of positive Iba-1+ cells [(F = 96.10, CCH 4w vs. sham, P < 0.01; CCH 4w vs. CCH 4w +APN-P, P < 0.01), (F = 234.43, CCH 8w vs. sham, P < 0.01; CCH 8w vs.

CCH 8w +APN-P, P < 0.01), (F = 300.24, CCH 12w vs. sham, P < 0.01; CCH 12w vs. CCH 12w +APN-P, P < 0.01)] and the microglial morphologies (**Fig. 2d–f**). Furthermore, we observed that APN-P treatment decreased the number of CD16+ microglia cells [(F = 118.48, CCH 4w vs. sham, P < 0.01; CCH 4w vs. CCH 4w +APN-P, P < 0.01), (F = 521.70, CCH 8w vs. sham, P < 0.01; CCH 8w vs. CCH 8w +APN-P, P < 0.01), (F = 151.54, CCH 12w vs. sham, P < 0.01; CCH 12w vs. CCH 12w +APN-P, P < 0.01)] and increased the number of CD206+ microglia cells [(F = 84.45, CCH 4w vs. sham, P < 0.01; CCH 4w vs. CCH 4w +APN-P, P < 0.01), (F = 330.95, CCH 8w vs. sham, P < 0.01; CCH 8w vs. CCH 8w +APN-P, P < 0.01), (F = 377.84, CCH 12w vs. sham, P < 0.01; CCH 12w vs. CCH 12w +APN-P, P < 0.01)] (**Fig. 2d, e, g, h**). Subsequently, the ratio of CD16/CD206 and CD206/CD16 were statistically analyzed to better understand the dynamic changes in microglial polarization. A ratio of CD16/CD206 higher than 1 indicates microglial polarization toward the M1 phenotype, while a ratio of CD206/CD16 higher than 1 indicates microglial polarization toward the M2 phenotype [12]. The data showed that the CD16/CD206 ratio increased 4 weeks after CCH and reached its highest value at 12 weeks compared to the sham condition [CCH 4w vs. sham, 2.94±0.91 vs. 1.08±0.14, P = 0.013; CCH 8w vs. sham, 3.93±0.53 vs. 1.08±0.14, P < 0.01; CCH 12w vs. sham, 4.89±0.72 vs. 1.08±0.14, P < 0.01] (**Fig. 2i**). However, CCH rats that received APN-P treatment had an increased CD206/CD16 ratio compared to CCH rats that did not receive APN-P [CCH 4w +APN-P vs. CCH 4w, 2.00±0.50 vs. 0.33±0.07, P < 0.01; CCH 8w +APN-P vs. CCH 8w, 3.67±0.29 vs. 0.26±0.03, P < 0.01; CCH 12w +APN-P vs. CCH 12w, 3.17±0.29 vs. 0.21±0.03, P < 0.01] (**Fig. 2j**).

To further verify that microglial polarization was associated with the M1 or M2 phenotype after CCH or APN-P treatment, qRT-PCR analysis was performed using different microglial markers to

assess the status of the M1 and M2 phenotypes. We found that APN-P treatment significantly reversed the CCH-induced upregulation of inflammatory cytokines (*iNOS, IL -6, IL-18, IL-1β,* and *TNF-α*) [(*iNOS*, $P < 0.01$), *(IL -6*, $P < 0.01$), (*IL-18*, $P < 0.01$), (*IL-1β*, $P < 0.01$), (*TNF-α*, $P < 0.01$)] (**Fig. 3a–e**) and the downregulation of anti-inflammatory cytokines (*Arg-1, IL-10*, and *TGF-β*) [(*Arg-1*, $P < 0.01$), (*IL-10*, $P < 0.01$), (*TGF-β*, $P < 0.01$)] in cortex (**Fig. 3f–h**). These results suggested that CCH induced microglial polarization toward the M1 phenotype, while APN-P treatment induced microglial polarization toward the M2 phenotype.

LPS is a strong stimulator of microglial activation, BV2 cells activated by LPS can act as an *in vitro* neuroinflammation model (LPS-BV2 cells) [26]. Using this model, the co-localization of the M1-associated marker CD16 or the M2-associated marker CD206 with Iba-1 was assessed using double-immunofluorescence staining (**Fig. 4a–b**). Compared to the control group, the numbers of both microglial phenotypes gradually increased in the LPS stimulation group, especially those for CD16+ microglia [$F = 196.00$, Control vs. APN-P, $P > 0.05$; Control vs. LPS, $P < 0.01$; LPS vs. LPS+APN-P, $P < 0.01$]. Conversely, APN-P treatment decreased the number of CD16+ microglia but increased the number of CD206+ microglia when compared to the control group [$F = 232.87$, Control vs. APN-P, $P < 0.01$; Control vs. LPS, $P = 0.087$; LPS vs. LPS+APN-P, $P < 0.01$] (**Fig. 4c-d**). In addition, the ratio of CD16/CD206 was higher than 1 in the LPS-stimulated BV2 cells [$F = 121.17$, Control vs. APN-P, 0.54±0.04 vs. 0.32±0.03, $P > 0.05$; Control vs. LPS, 0.54±0.04 vs. 2.97±0.38, $P < 0.01$; LPS vs. LPS+APN-P, 2.97±0.38 vs. 0.70±0.04, $P < 0.01$] (**Fig. 4e**), while the CD206/CD16 ratio was higher than 1 in the APN-P-treated LPS-BV2 cells [$F = 107.99$, Control vs. APN-P, 1.86±0.16 vs. 3.11±0.03, $P < 0.01$; Control vs. LPS, 1.86±0.16 vs. 0.34±0.04, $P < 0.01$; LPS vs. LPS+APN-P, 0.34±0.04 vs. 1.43±0.07, $P < 0.01$] (**Fig. 4f**). These results also

indicated that APN-P treatment induced microglial polarization toward the M2 phenotype under environment of neuroinflammation *in vitro*.

APN-P promotes microglial polarization toward the M2 phenotype through inhibition of the NF-κB pathway

We detected p-NF-κB expression levels to further investigate whether the effect of APN-P on microglial polarization was mediated by NF-κB pathway. The ratio of p-NF-κB/NF-κB significantly increased in the cortex of the CCH rats, while APN-P treatment significantly reduced this ratio [(F =68.66, CCH 4w vs. sham, $P < 0.01$; CCH 4w vs. CCH 4w +APN-P, $P < 0.01$), (F = 307.90, CCH 8w vs. sham, $P < 0.01$; CCH 8w vs. CCH 8w +APN-P, $P < 0.01$), (F = 98.89, CCH 12w vs. sham, $P < 0.01$; CCH 12w vs. CCH 12w +APN-P, $P < 0.01$)] (**Fig. 5a–b**). These results showed that APN-P had an inhibitory effect on the NF-κB pathway *in vivo*. However, we found that APN-P treatment could inhibit the expression of p-NF-κB in LPS-activated BV2 cells (F = 12.99, Control vs. LPS, P = 0.015; LPS vs. LPS+APN-P, P = 0.049), which was due to the effect of the p-NF-κB inhibitor, BAY in in the BV2 cells (LPS vs. LPS+BAY, $P < 0.01$) (**Fig. 5c–d**). In addition, when p-NF-κB was suppressed, the relative level of the M1 marker iNOS decreased (F = 244.43, Control vs. LPS, $P < 0.01$; LPS vs. LPS+BAY, $P < 0.01$; LPS vs. LPS+APN-P, $P < 0.01$); however, the M2 marker Arg-1 increased (F = 46.39, Control vs. LPS, $P < 0.01$; LPS vs. LPS+BAY, $P < 0.01$; LPS vs. LPS+APN-P, P = 0.037) with APN-P treatment in LPS-BV2 cells compared to the LPS treatment alone (**Fig. 5c–d**). Moreover, when p-NF-κB was suppressed, the expression of pro-inflammatory factors (*iNOS*, *IL-6*, *IL-18*, *IL-1β*, and *TNF-α*) were decreased [(*iNOS*, $P < 0.01$), (*IL -6*, $P < 0.01$), (*IL-18*, $P < 0.01$), (*IL-1β*, $P < 0.01$), (*TNF-α*, $P <$

0.01)] (**Fig. 5e–i**), while that of anti-inflammatory factors (*Arg-1*, *IL-10*, and *TGF-β*) were increased in both BAY- and APN-P-treated LPS-BV2 cells [(*Arg-1*, $P < 0.01$), (*IL-10*, $P < 0.01$), (*TGF-β*, $P < 0.01$)] (**Fig. 5j–m**). These results indicated that APN-P promoted microglial polarization toward the M2 phenotype through the inhibition of the NF-κB pathway.

The effects of APN-P on neuron protection in CCH rats and LPS-BV2 cells

When we used Nissl staining to evaluate neuron protection effect of APN-P, we found that compared to the CCH group, APN-P treatment significantly alleviated neuron damage in the cortex [CCH 4w+APN-P vs. CCH 4w, $F = 272.74$, $P < 0.01$; CCH 8w+APN-P vs. CCH 8w, $F = 268.94$, $P < 0.01$; CCH 12w+APN-P vs. CCH 12w, $F = 1080.41$, $P < 0.01$] (**Fig. 6a, b**) and the CA1 region of the hippocampus [CCH 4w+APN-P vs. CCH 4w, $F = 350.98$, $P < 0.01$; CCH 8w+APN-P vs. CCH 8w, $F = 126.90$, $P < 0.01$; CCH 12w+APN-P vs. CCH 12w, $F = 282.12$, $P < 0.01$] (**Fig. 6a, c**). These results indicated that APN-P treatment had neuroprotective effects against CCH. To further determine whether the neuron protection effects of APN-P on microglia altered neuron viability in a neuroinflammation environment (i.e., LPS treatment), we constructed a microglia-neuron co-culture system to mimic the coexistence of microglia cells and cortex/hippocampal neurons *in vitro* (**Fig. 6d**). As shown in **Fig. 6e**, the viabilities of primary cortical neurons decreased in the LPS-treated group, in which neurons were cultured by medium from LPS-treated BV2 cells. Indeed, in groups treated with medium from LPS-treated BV2 cells supplemented with BAY and APN-P, neuron viability was significantly increased, although they did not return to normal levels [$F = 162.28$, Control vs. LPS, 100.08%±1.60 vs. 72.46%±0.98, $P < 0.01$; LPS+BAY vs. LPS, 85.74%±1.88 vs. 72.46%±0.98, $P < 0.01$; LPS+APN-P vs. LPS, 86.07%±2.94 vs. 72.46%±0.98,

P < 0.01]. We further found that medium from LPS-treated BV2 cells supplemented with BAY and APN-P increased the number of CMFDA-positive hippocampal HT-22 cells, indicating improved cell viability in comparison to the LPS-treated BV2 cells [F = 176.87, Control vs. LPS, 154.43±2.03 vs. 76.58±6.10, P < 0.01; LPS+BAY vs. LPS, 149.54±4.31 vs. 76.58±6.10, P < 0.01; LPS+APN-P vs. LPS, 146.86±5.74 vs. 76.58±6.10, P < 0.01] (**Fig. 6f–g**).

These results confirmed that in addition to reducing neuron death, APN-P supplementation could effectively decrease damage of primary cortical neurons and hippocampal HT-22 cell viability induced by LPS-BV2 cell neuroinflammation.

APN-P improves learning and memory function in CCH rats

Using the Morris water maze test, we showed that APN-P treatment improved learning, which was indicated by a decreased EL [(Day 1, F = 4.89, P > 0.01), (Day 2, F = 12.99, P < 0.01), (Day 3, F = 75.66, P < 0.01), (Day 4, F = 84.68, P < 0.01), (Day 5, F = 73.09, P < 0.01)] (**Fig. 7a**) and memory function, which was indicated by an increased frequency of platform crossing (F = 56.78, sham vs. CCH, P < 0.01, CCH + APN-P vs. CCH, P < 0.01) and residence time in the target quadrant (F = 84.99, sham vs. CCH, P < 0.01, CCH + APN-P vs. CCH, P < 0.01) compared to the CCH group (**Fig. b–c**). Representative images of frequency of platform crossing in different groups are displayed in **Fig. 7d**. These results indicated that APN-P treatment could improve cognitive function in CCH rats.

Discussion

CCH is a widespread condition observed in central nervous system diseases and commonly

accompanied by cognitive impairment. Therefore, developing targeted therapeutic strategies to improve cognitive function are of great significance to the outcome of individuals with CCH. The major findings of the present research can be summarized as follows: **(a)** CCH presents confounding pathological features including cognitive impairment, neuronal damage, microglial activation that mediates neuroinflammation, M1-type polarization, and exacerbated activation of NF-κB signaling. **(b)** APN-P treatment might be a novel therapeutic strategy for CCH, evidenced by the increased neuronal survival and improved neurological function observed in CCH mice treated with APN-P when compared to the CCH control group. **(c)** APN-P treatment alleviated neuroinflammation and promoted microglia M2-type polarization after CCH and LPS stimulation. **(d)** Mechanistically, the positive APN-P effect on CCH-associated neuronal dysfunction and damage was NF-κB signaling-dependent.

In addition to its known function in the maintenance of metabolic homoeostasis, APN possesses anti-inflammatory, antioxidant, and antiatherogenic properties [16]. The concentration of plasma APN declines is inversely correlated with poor outcomes of acute neural injury [16]. A previous report showed that APN protected against glutamate-induced excitotoxicity in nervous system-related diseases [27]. In an animal model for cerebral ischemia-reperfusion injury, APN attenuated oxidative stress and neuronal damage [17]. Additionally, APN ameliorated brain injury by suppressing astrocyte-derived inflammation following intracerebral hemorrhage [23]. Thus, there is considerable evidence that supports the direct and indirect influence of APN on β-amyloid and tau aggregate formation; thus, elevation of APN levels might constitute a neuroprotective strategy in AD [28]. APN is a classic anti-inflammatory agent in multiple systems including the cardio-cerebrovascular system via reducing inflammation and switching the macrophage phenotype

475 to an anti-inflammatory state [15]. These studies suggest that reduced APN function plays a
476 causative role in neurological impairment after CCH, which inspired us to hypothesize that
477 exogenous supplementation of APN could be a promising therapeutic strategy, although the role of
478 APN in CCH is unclear.

479 Intracerebroventricular injection has been the primary method adopted for drug delivery [2];
480 however, this method can lead to cerebral injury and may not be suitable for clinical practice.
481 Because the full-length APN has restricted blood-brain barrier permeability that reduces its potential
482 for future clinical applications, a recombinant APN-P was synthetized [16, 23] and used in the
483 present study. We found that APN-P significantly improved the cognitive function, attenuated
484 microglial activation, and mediated neuroinflammation and neuronal survival in the rat
485 cortex/hippocampus. These findings highlight the promising neuroprotective effects of APN-P
486 treatment on CCH in human patients.

487 Previous study has suggested that neuroinflammation plays a crucial role in the cognitive
488 dysfunction induced by CCH [29]. Microglia are resident immune cells of the central nervous
489 system that maintain brain homeostasis. A previous study reported that neuroinflammation is mainly
490 manifested by microglial activation and the subsequent release of inflammatory factors, which lead
491 to brain damage ultimately [30]. In this study, we also found that microglia activation accompanied
492 CCH in the cortex. Neuron death is a key hallmark of CCH-related cognitive impairment [7], and it
493 is well established that inflammatory responses induced by CCH, including the activation of glial
494 cells and inflammatory cytokine production, could further result in neuron death and cognitive
495 deficits [30]. In addition, we found that microglia activation was accompanied by neuronal damage
496 in the cortex of CCH rats in this study. Therefore, inhibiting microglial activation to the pro-

497 inflammatory phenotype could alleviate neuronal injury [29].

498 Activated microglia represent a variety of phenotypes after injury, including the broadly
499 classified M1 and M2 phenotypes that are useful for understanding the function and effect of
500 microglia in diversiform brain diseases [12]. The M2-to-M1 phenotypic changes during chronic
501 inflammation may be regulated by a common pathologic mechanism that underlies multiple types
502 of injuries in the central nervous system, including traumatic brain injury, white matter lesions,
503 spinal cord injuries, and strokes [31]. These dynamic phenotypic changes observed in brain diseases
504 suggest that manipulating microglial polarization might be a promising therapeutic strategy with
505 neuroprotective effects. However, research on the underlying mechanism and related potential
506 interventions of microglial polarization during CCH are currently limited. We used three methods
507 to evaluate how CCH affects the microglial polarization process. First, we detected increased iNOS
508 and decreased Arg-1 protein levels in the cortexes of CCH rats compared to sham controls. Second,
509 immunofluorescence was used to evaluate Iba-1, CD16, and CD206 expression as biomarkers for
510 microglial polarization. We found that the ratio of CD16/CD206 in Iba-1+ cells in the cortex of
511 CCH rats gradually increased between 4 and 12 weeks after BCCAO surgery. Third, microglial
512 polarization was further shown to significantly increase the mRNA levels of *iNOS*, *IL-6*, *IL-18*, *IL-*
513 *1β*, and *TNF-α* in CCH groups compared to those in the sham control. These results demonstrated
514 that during CCH, the microglia switched towards an M1 phenotype, which is associated with
515 neuroinflammation. Conversely, APN-P treatment in CCH rats promoted the microglia towards the
516 detrimental M2 phenotype, with decreased *iNOS* and increased *Arg-1* expression, an increased
517 CD206/CD16 ratio in Iba-1+ cells, and secretion of anti-inflammatory factors.

518 Research have focused on the role of the hippocampus in cognitive impairment, but spatial

519 reference memory is thought to be related to the integrity of both the hippocampus and cortex [32].
520 The onset of CCH is in the associative cortical areas; then, it spreads throughout the brain via the
521 neuronal network, affecting cognitive function [33]. Our previous studies also showed that CCH
522 resulted in hypoperfusion of cortical cerebral blood flow in rats, as well as white matter fiber injury
523 and neuron death in the cortex [7, 9]. Considering cerebral white matter is comprised of nerve fibers
524 that interconnect neurons in the cortex or the deep structures [34], pathological changes in the
525 cerebral cortex caused by CCH could also be associated with cognitive impairment. Therefore, we
526 focused on the CCH effects on cortex in this study. We found APN-P not only regulated microglial
527 polarization changes in the cortex of CCH rats but also showed a protective effect on cortical and
528 hippocampal neurons *in vivo*. *In vitro* results also indicated a neuroprotective effect in the two
529 neuronal cell lines when co-cultured with activated BV2 microglia cells. Together, these results
530 indicated that APN-P treatment could reduce cortex injury through the mediation of pro- and anti-
531 inflammatory responses that contribute to CCH tissue damage, further suggesting a therapeutic
532 potential for ANP-P treatment strategies for cortex injuries.

533 CCH causes a cascade of pathological processes during which diverse signaling pathways are
534 activated [30]. Our *in vivo* study found that CCH could activate the NF-κB signaling pathways,
535 which are closely related to neuroinflammation [35] and can induce the production of pro-
536 inflammatory molecules that promote apoptosis in neural cells and cause secondary neurotoxicity
537 [36]. A previous study indicated that APN inhibits ROS-induced cardiac remodeling in rat
538 ventricular myocytes by inhibiting NF-κB activation and that APN mediates the suppression of NF-
539 κB activation and pro-inflammatory cytokine expression, leading to a suppression of M1
540 macrophage proliferation and function [15]. Consistent with these previous findings, we observed

that APN-P could efficiently inhibit NF-κB activation in the cortex of CCH rats, and our *in vitro* results from LPS-activated BV2 microglial cells showed that an NF-κB inhibitor and and APN-P treatment could mediate the suppression of M1 polarization and pro-inflammatory factor expression. Consistent with the effect of the NF-κB inhibitor, APN-P mediated the promotion of M2 polarization and anti-inflammatory factor expression in LPS-induced BV2 cells.

This study has several limitations. First, APN-P-mediated protection after CCH was studied using a single dose concentration; future studies should assess concentration-dependent effects of APN-P. Second, we focused on changes in microglial cells after CCH and APN-P treatment, but the potential effects on microglia-neuron crosstalk deserve further exploration. Third, exploration of the effects of APN-P on CCH in aging, diabetes, or obesity is warranted in follow-up studies due to the vital role of APN in metabolic regulation. Finally, none of the experimental CCH models currently in use can completely mimic the clinical CCH process, and before clinical application, the translational challenges of this novel treatment must be fully considered.

Conclusions

Collectively, APN downregulation is involved in CCH-induced polarization of cortex microglia toward the pro-inflammatory M1 phenotype. APN-P showed neuroprotective effects against neuron damage after CCH, which alleviated microglia-derived inflammation and regulated the transformation of microglial cells to the anti-inflammatory M2 phenotype. These effects were mediated by the suppression of NF-κB signaling. This study provides a novel and potentially therapeutic strategy for future clinical application of APN-P in the treatment of CCH-induced cognitive impairment in human patients.

Abbreviations

CCH, Chronic cerebral hypoperfusion; APN, Adiponectin; APN-P, Recombinant adiponectin peptide; BCCAO, Bilateral common carotid artery occlusion; CBF, Cerebral blood flow; LPS, Lipopolysaccharide; qRT-PCR, Quantitative reverse transcription polymerase chain reaction; BAY, BAY 11-7082; EL, Escape latency; RIPA, Radio-Immunoprecipitation Assay; SDS-PAGE, sodium dodecyl sulfatepolyacrylamide gel; PVDF, polyvinylidene difluoride; TBST, Tris-buffered saline and Tween-20; Arg-1, Arginase-1; IL-6, Interleukin-6; IL-18, Interleukin-18; IL-1β, Interleukin-1β; TNF-α, Tumor necrosis factor-α; IL-10, Interleukin-10; TGF-β, Transforming growth factor-β; ROS, Reactive oxygen species; ROI, Region of interest for quantitative analysis.

Ethics approval and consent to participate

All protocols were approved by the Animal Care and Use Committee of Xi'an Jiaotong University and conformed to the Guide for the Care and Use of Laboratory Animals by the National Institutes of Health, USA.

Consent for publication

Not applicable.

Availability of data and materials

The datasets generated and/or analyzed in the current study are available from the corresponding author on reasonable request.

Competing interests

The authors declare that they have no competing interests.

Funding

This work was supported by the National Natural Science Foundation of China (No. 81971120, No. 81971116), the National Natural Science Foundation of Guangdong province (No. 2018A0303130264), and the Shaanxi Science Research Project (No. 2019ZDLSF01-04), China.

Authors' contributions

Wenxian Li, Di Wei and Zheng Zhu wrote the paper and performed the most of experiments. Shuqin Zhan, Ru Zhang and Huqing Wang collected and analyzed the data. Guilian Zhang and Li'an Huang designed the research and revised the manuscript.

Acknowledgments

We thank the support from the Department of Neurology, The Second Affiliated Hospital, Xi'an Jiaotong University, and the First Affiliated Hospital, Jinan University. Thanks to Editage® for editing and polishing the manuscript.

Author details

[1] Department of Neurology, The Second Affiliated Hospital, Xi'an jiaotong University, Xi'an, Shanxi, China.

[2] Department of Urology, Xijing Hospital, The Fourth Military Medical University, Xi'an, Shanxi, China.

[3] Department of Internal Medicine, Division of Hematology/Oncology, University of California Davis, Sacramento, CA 95817, USA.

[4] Department of Neurology, The First Affiliated Hospital, Jinan University, Guangzhou, Guangdong, China.

Reference

1. Liu Q, Radwanski R, Babadjouni R, Patel A, Hodis DM, Baumbacher P, Zhao Z, Zlokovic B and Mack WJ. Experimental chronic cerebral hypoperfusion results in decreased pericyte coverage and increased blood-brain barrier permeability in the corpus callosum. Journal of cerebral blood flow and metabolism : official journal of the International Society of Cerebral Blood Flow and Metabolism. 2019; 39(2):240-250.
2. Fang C, Li Q, Min G, Liu M, Cui J, Sun J and Li L. MicroRNA-181c Ameliorates Cognitive Impairment Induced by Chronic Cerebral Hypoperfusion in Rats. Molecular neurobiology. 2017; 54(10):8370-8385.
3. Zou W, Song Y, Li Y, Du Y, Zhang X and Fu J. The Role of Autophagy in the Correlation Between Neuron Damage and Cognitive Impairment in Rat Chronic Cerebral Hypoperfusion. Molecular neurobiology. 2018; 55(1):776-791.
4. Du SQ, Wang XR, Xiao LY, Tu JF, Zhu W, He T and Liu CZ. Molecular Mechanisms of Vascular Dementia: What Can Be Learned from Animal Models of Chronic Cerebral Hypoperfusion? Molecular neurobiology. 2017; 54(5):3670-3682.
5. Su SH, Wu YF, Lin Q, Wang DP and Hai J. URB597 protects against NLRP3 inflammasome activation by inhibiting autophagy dysfunction in a rat model of chronic cerebral hypoperfusion. Journal of neuroinflammation. 2019; 16(1):260.
6. Ren C, Li N, Li S, Han R, Huang Q, Hu J, Jin K and Ji X. Limb Ischemic Conditioning Improved Cognitive Deficits via eNOS-Dependent Augmentation of Angiogenesis after Chronic Cerebral Hypoperfusion in Rats. Aging and disease. 2018; 9(5):869-879.
7. Li W, Wei D, Lin J, Liang J, Xie X, Song K and Huang L. Dl-3-n-Butylphthalide Reduces Cognitive Impairment Induced by Chronic Cerebral Hypoperfusion Through GDNF/GFRalpha1/Ret Signaling Preventing Hippocampal Neuron Apoptosis. Frontiers in cellular neuroscience. 2019; 13:351.
8. Song D, Zhang X, Chen J, Liu X, Xue J, Zhang L and Lan X. Wnt canonical pathway activator TWS119 drives microglial anti-inflammatory activation and facilitates neurological recovery following experimental stroke. Journal of neuroinflammation. 2019; 16(1):256.
9. Li W, Wei D, Liang J, Xie X, Song K and Huang L. Comprehensive Evaluation of White Matter

643 Damage and Neuron Death and Whole-Transcriptome Analysis of Rats With Chronic Cerebral
644 Hypoperfusion. Frontiers in cellular neuroscience. 2019; 13:310.
645 10. Chen X, Jiang XM, Zhao LJ, Sun LL, Yan ML, Tian Y, Zhang S, Duan MJ, Zhao HM, Li WR, Hao
646 YY, Wang LB, Xiong QJ and Ai J. MicroRNA-195 prevents dendritic degeneration and neuron death
647 in rats following chronic brain hypoperfusion. Cell death & disease. 2017; 8(6):e2850.
648 11. Nishio K, Ihara M, Yamasaki N, Kalaria RN, Maki T, Fujita Y, Ito H, Oishi N, Fukuyama H,
649 Miyakawa T, Takahashi R and Tomimoto H. A mouse model characterizing features of vascular
650 dementia with hippocampal atrophy. Stroke. 2010; 41(6):1278-1284.
651 12. Mao M, Xu Y, Zhang XY, Yang L, An XB, Qu Y, Chai YN, Wang YR, Li TT and Ai J. MicroRNA-
652 195 prevents hippocampal microglial/macrophage polarization towards the M1 phenotype
653 induced by chronic brain hypoperfusion through regulating CX3CL1/CX3CR1 signaling. Journal of
654 neuroinflammation. 2020; 17(1):244.
655 13. Chi GC, Fitzpatrick AL, Sharma M, Jenny NS, Lopez OL and DeKosky ST. Inflammatory
656 Biomarkers Predict Domain-Specific Cognitive Decline in Older Adults. The journals of
657 gerontology Series A, Biological sciences and medical sciences. 2017; 72(6):796-803.
658 14. Liu R, Liao XY, Pan MX, Tang JC, Chen SF, Zhang Y, Lu PX, Lu LJ, Zou YY, Qin XP, Bu LH and
659 Wan Q. Glycine Exhibits Neuroprotective Effects in Ischemic Stroke in Rats through the Inhibition
660 of M1 Microglial Polarization via the NF-kappaB p65/Hif-1alpha Signaling Pathway. Journal of
661 immunology (Baltimore, Md : 1950). 2019; 202(6):1704-1714.
662 15. Fang H and Judd RL. Adiponectin Regulation and Function. Comprehensive Physiology. 2018;
663 8(3):1031-1063.
664 16. Wu X, Luo J, Liu H, Cui W, Guo W, Zhao L, Guo H, Bai H, Guo K, Feng D and Qu Y. Recombinant
665 adiponectin peptide promotes neuronal survival after intracerebral haemorrhage by suppressing
666 mitochondrial and ATF4-CHOP apoptosis pathways in diabetic mice via Smad3 signalling
667 inhibition. Cell proliferation. 2020; 53(2):e12759.
668 17. Li X, Guo H, Zhao L, Wang B, Liu H, Yue L, Bai H, Jiang H, Gao L, Feng D and Qu Y. Adiponectin
669 attenuates NADPH oxidase-mediated oxidative stress and neuronal damage induced by cerebral
670 ischemia-reperfusion injury. Biochimica et biophysica acta Molecular basis of disease. 2017;
671 1863(12):3265-3276.
672 18. Wang B, Guo H, Li X, Yue L, Liu H, Zhao L, Bai H, Liu X, Wu X and Qu Y. Adiponectin Attenuates
673 Oxygen-Glucose Deprivation-Induced Mitochondrial Oxidative Injury and Apoptosis in
674 Hippocampal HT22 Cells via the JAK2/STAT3 Pathway. Cell transplantation. 2018; 27(12):1731-
675 1743.
676 19. Huang TF, Tang ZP, Wang S, Hu MW, Zhan L, Yi Y, He YL and Cai ZY. Decrease in Serum
677 Levels of Adiponectin and Increase in 8-OHdG: a Culprit for Cognitive Impairment in the Elderly
678 Patients with Type 2 Diabetes. Current molecular medicine. 2019; 20(1):44-50.
679 20. Efstathiou SP, Tsioulos DI, Tsiakou AG, Gratsias YE, Pefanis AV and Mountokalakis TD. Plasma
680 adiponectin levels and five-year survival after first-ever ischemic stroke. Stroke. 2005; 36(9):1915-
681 1919.
682 21. Wu X, Luo J, Liu H, Cui W, Guo K, Zhao L, Bai H, Guo W, Guo H, Feng D and Qu Y. Recombinant
683 Adiponectin Peptide Ameliorates Brain Injury Following Intracerebral Hemorrhage by Suppressing
684 Astrocyte-Derived Inflammation via the Inhibition of Drp1-Mediated Mitochondrial Fission.
685 Translational stroke research. 2020.
686 22. Sun H, Chen GY and Yao SQ. Recent advances in microarray technologies for proteomics.

687 Chemistry & biology. 2013; 20(5):685-699.
688 23. Wu X, Luo J, Liu H, Cui W, Guo K, Zhao L, Bai H, Guo W, Guo H, Feng D and Qu Y. Recombinant
689 Adiponectin Peptide Ameliorates Brain Injury Following Intracerebral Hemorrhage by Suppressing
690 Astrocyte-Derived Inflammation via the Inhibition of Drp1-Mediated Mitochondrial Fission.
691 Translational stroke research. 2020; 11(5):924-939.
692 24. Li W, Wei D, Xie X, Liang J, Song K and Huang L. Dl-3-n-Butylphthalide regulates the Ang-
693 1/Ang-2/Tie-2 signaling axis to promote neovascularization in chronic cerebral hypoperfusion.
694 Biomedicine & pharmacotherapy = Biomedecine & pharmacotherapie. 2019; 113:108757.
695 25. Zhang Z, Qin P, Deng Y, Ma Z, Guo H, Hou Y, Wang S, Zou W, Sun Y, Ma Y and Hou W. The
696 novel estrogenic receptor GPR30 alleviates ischemic injury by inhibiting TLR4-mediated microglial
697 inflammation. Journal of neuroinflammation. 2018; 15(1):206.
698 26. Nam HY, Nam JH, Yoon G, Lee JY, Nam Y, Kang HJ, Cho HJ, Kim J and Hoe HS. Ibrutinib
699 suppresses LPS-induced neuroinflammatory responses in BV2 microglial cells and wild-type mice.
700 Journal of neuroinflammation. 2018; 15(1):271.
701 27. Yue L, Zhao L, Liu H, Li X, Wang B, Guo H, Gao L, Feng D and Qu Y. Adiponectin Protects
702 against Glutamate-Induced Excitotoxicity via Activating SIRT1-Dependent PGC-1α Expression in
703 HT22 Hippocampal Neurons. Oxidative medicine and cellular longevity. 2016; 2016:2957354.
704 28. Letra L, Rodrigues T, Matafome P, Santana I and Seiça R. Adiponectin and sporadic
705 Alzheimer's disease: Clinical and molecular links. Frontiers in neuroendocrinology. 2019; 52:1-11.
706 29. Zhang LY, Pan J, Mamtilahun M, Zhu Y, Wang L, Venkatesh A, Shi R, Tu X, Jin K, Wang Y,
707 Zhang Z and Yang GY. Microglia exacerbate white matter injury via complement C3/C3aR pathway
708 after hypoperfusion. Theranostics. 2020; 10(1):74-90.
709 30. Zhang J, Liu Y, Zheng Y, Luo Y, Du Y, Zhao Y, Guan J, Zhang X and Fu J. TREM-2-p38 MAPK
710 signaling regulates neuroinflammation during chronic cerebral hypoperfusion combined with
711 diabetes mellitus. Journal of neuroinflammation. 2020; 17(1):2.
712 31. Wang LY, Tao Z, Zhao HP, Wang RL, Li LZ, Luo YM and Chen ZG. Huoluo Yinao decoction
713 mitigates cognitive impairments after chronic cerebral hypoperfusion in rats. Journal of
714 ethnopharmacology. 2019; 238:111846.
715 32. Block F and Schwarz M. Correlation between hippocampal neuronal damage and spatial
716 learning deficit due to global ischemia. Pharmacology, biochemistry, and behavior. 1997;
717 56(4):755-761.
718 33. Völgyi K, Gulyássy P, Todorov MI, Puska G, Badics K, Hlatky D, Kékesi KA, Nyitrai G, Czurkó A,
719 Drahos L and Dobolyi A. Chronic Cerebral Hypoperfusion Induced Synaptic Proteome Changes in
720 the rat Cerebral Cortex. Molecular neurobiology. 2018; 55(5):4253-4266.
721 34. Tomimoto H. White matter integrity and cognitive dysfunction: Radiological and
722 neuropsychological correlations. Geriatrics & gerontology international. 2015; 15 Suppl 1:3-9.
723 35. Shih RH, Wang CY and Yang CM. NF-kappaB Signaling Pathways in Neurological
724 Inflammation: A Mini Review. Frontiers in molecular neuroscience. 2015; 8:77.
725 36. Li B, Dasgupta C, Huang L, Meng X and Zhang L. MiRNA-210 induces microglial activation
726 and regulates microglia-mediated neuroinflammation in neonatal hypoxic-ischemic
727 encephalopathy. Cellular & molecular immunology. 2020; 17(9):976-991.
728
729
730

Figure Legends

Fig. 1 Microglial activation and decreased expression of APN in the cortex of CCH rats.

a. A flowchart of the animal experiments.

b. Representative images of Iba-1+ and NeuN+ cells in the cortexes of sham and CCH rats at the 2^{nd}, 4^{th}, 8^{th}, and 12^{th} week after BCCAO surgery. Magnification ×20, scale bar = 100 μm.

c. Quantification of the Iba-1+ cells in the cortex region of rats in different groups.

d. There was a negative correlation between the Iba-1+ and NeuN+ cell numbers.

Values are mean ± SD, n = 3 slices from 4 animals per group, *P < 0.05, **P < 0.01 vs sham group, Student's t test and Pearson correlation analysis. ROI, 200μm^2.

e. A heat map representation of the protein level analysis of antibody arrays that show that APN was the most statistically significant among 10 proteins in the cortex of CCH 12w rats compared to the sham (fold change = -4.23, P < 0.05; n = 6 animals per group).

f. Representative images of APN expression in Iba-1+ cells in the cortex region of sham and CCH rats at the 12^{th} week after BCCAO surgery. Magnification ×60, scale bar = 30 μm.

g. Quantification of the ratio of APN in Iba-1+ cells in cortex region.

Values are mean ± SD, n = 3 slices from 3 animals per group, **P < 0.01 vs sham group, Student's t test. ROI, 100μm^2.

Fig. 2 CCH polarizes microglia toward M1 phenotypes, while APN-P promotes M2 phenotypes in the rat cortex

a. The amino acid sequence of APN-P [23].

b, c. Western blotting analysis of the relative protein levels of APN, iNOS, and Arg-1 expressed *in*

753 *vivo*.

754 **d.** Representative images of CD16 expression in Iba-1+ cells in the cortex of sham, CCH, and CCH

755 rats with APN-P treatment groups. Magnification ×60, scale bar = 30 μm.

756 **e.** Representative images of CD206 expression in Iba-1+ cells in cortex of sham, CCH and, CCH

757 with APN-P treatment groups. Magnification ×60, scale bar = 30 μm.

758 **f.** Quantification of the Iba-1+ cell number in the cortex of different treatment groups.

759 **g.** Quantification of CD16 in Iba-1+ cells (%) in the cortex of different treatment groups.

760 **h.** Quantification of CD206 in Iba-1+ cells (%) in the cortex of different groups.

761 **i.** Quantification of the CD16/CD206 ratio in the cortex of different treatment groups.

762 **j.** Quantification of the CD206/CD16 ratio in the cortex of different treatment groups.

763 Values are mean ± SD, n = 3 slices from 3 animals per group, **P < 0.01 CCH vs sham groups, ##P

764 < 0.01 CCH+APN-P vs CCH groups, One way ANOVA test, Tukey tests. ROI, 100μm^2.

765

766 **Fig. 3 CCH induces inflammatory responses, while APN-P treatment induces anti-**

767 **inflammatory responses in the rat cortex**

768 The mRNA expression of (**a**) *iNOS*, (**b**) *IL-6*, (**c**) *IL-18*, (**d**) *IL-1β*, (**e**) *TNF-α*, (**f**) *Arg-1*, (**g**) *IL-10*,

769 and (**h**) *TGF-β* in the cortex of rats in different groups. Values are mean ± SD, n = 6 animals per

770 group, **P < 0.01 CCH vs sham groups, ##P < 0.01 CCH+APN-P vs CCH groups, One way

771 ANOVA test, Tukey tests.

772

773 **Fig. 4 APN-P promotes the microglia M2 phenotype in LPS-induced BV2 cells**

774 Representative immunofluorescent images of (**a**) CD16 and (**b**) CD206 expression in Iba-1+ cells

775 in BV2 cells from control, LPS, and LPS+APN-P treatment groups. Magnification ×60, scale bar =

776 30 μm.

777 Quantification of (**c**) CD16 in Iba-1+ cells (%), (**d**) CD206 in Iba-1+ cells (%), (**e**) CD16/CD206

778 ratio, and (**f**) CD206/CD16 ratio in BV2 cells of different groups.

779 Values are mean ± SD, n = 3 slices from 3 animals per group, **P < 0.01 LPS vs control group, ##P

780 < 0.01 vs LPS group, One way ANOVA test, Tukey tests. ROI, 100μm^2.

781

782 **Fig. 5 APN-P promotes the microglial M2 phenotype and anti-inflammatory responses via NF-**

783 **κB pathway inhibition**

784 **a.** Western blotting analysis of *in vivo* NF-κB and p-NF-κB protein expression.

785 **b.** Quantification of the *in vivo* p-NF-κB/NF-κB ratio.

786 Values are mean ± SD, n = 3 samples per group, **P < 0.01 CCH vs sham group, ##P < 0.01

787 CCH+APN-P vs CCH group, One way ANOVA test, Tukey tests.

788 **c.** Western blotting analysis of the protein expression of NF-κB, p-NF-κB, iNOS and Arg-1 *in vivo*.

789 **d.** Quantification of the *in vitro* p-NF-κB/NF-κB ratio relative to iNOS and Arg-1 expression levels

790 in control, LPS treatment, LPS + BAY and LPS + APN-P treated groups.

791 Values are mean ± SD, n = 3 samples per group, *P < 0.05, **P < 0.01 LPS vs control group, #P <

792 0.05, ##P < 0.01 vs LPS group, One way ANOVA test, Tukey tests.

793 The mRNA expression of (**e**) *iNOS*, (**f**) *IL-6*, (**g**) *IL-18*, (**h**) *IL-1β*, (**i**) *TNF-α*, (**j**) *Arg-1*, (**k**) *IL-10*,

794 and (**m**) *TGF-β* in BV2 cells in different groups.

795 Values are mean ± SD, n = 6 samples per group, **P < 0.01 LPS vs control group, ##P < 0.01 vs

796 LPS group, One way ANOVA test, Tukey tests.

Fig. 6 Effects of APN-P on neuron protection

a. Sections of the cortex and the hippocampal CA1 region were obtained and treated with Nissl staining. Magnification ×40, scale bar = 50 μm.

b. Quantitative analysis of neuronal damage of the cortex region.

c. Quantitative analysis of neuronal damage of the hippocampal CA1 region.

Values are mean ± SD, n = 3 samples per group, **P < 0.01 CCH vs sham group, ##P < 0.01 CCH+APN-P vs CCH group, One way ANOVA test, Tukey tests. ROI, 200μm^2.

d. Flowchart of *in vitro* experiments (a microglia-neuron co-culture system).

e. Quantitative analysis of neuronal viability of BV2 cells from different groups after co-culturing using a CCK-8 test.

Values are mean ± SD, n = 5 samples per group, **P < 0.01 LPS vs control group, ##P < 0.01 vs LPS group, One way ANOVA test, Tukey tests.

f. Representative images of CMFDA-labeled neurons (green) after co-culturing with different BV2 cells. Magnification ×40, scale bar = 100 μm.

g. The quantification of the CMFDA fluorescence intensity in different groups.

Values are mean ± SD, n = 3 samples per group, **P < 0.01 LPS vs control group, ##P < 0.01 vs LPS group, One way ANOVA test, Tukey tests.

Fig. 7 CCH exacerbates cognitive deficits, while APN-P improved cognitive function in rats

a. EL of rats trained in a Morris water maze (day 1 to day 5).

Values are mean ± SD, n = 6 samples per group, **P < 0.01 CCH 4w vs sham group, ##P < 0.01

CCH 4w + APN-P vs CCH 4w group; **'P < 0.01 CCH 8w vs sham group, ##'P < 0.01 CCH 8w + APN-P vs CCH 8w group; **''P < 0.01 CCH 12w vs sham group, ##''P < 0.01 CCH 12w + APN-P vs CCH 12w group, Two-way ANOVA, Bonferroni *post hoc* test.

b. Number of platform location crosses indicating that the CCH and CCH+APN-P treatment groups were significantly different from each other on day 6.

c. Stay time of each treatment group on the platform during a single 60-s probe trial (day 6). Values are mean ± SD, n = 6 samples per group, **P < 0.01 CCH vs sham group, ##P < 0.01 CCH + APN-P vs CCH group, Two-way ANOVA, Bonferroni *post hoc* test.

d. Representative images of the number of platform location crosses of each treatment group in the Morris water maze.

Fig. 8 Graphical abstract

APN-P inhibited the NF-κB pathway and regulated microglial polarization from an M1 toward an M2 phenotype, which alleviated the inflammatory response and cortical neural injury, rescuing CCH-induced cognitive impairment.

Additional files

Additional file 1

Table S1. Animal groups and number of rats used in the research. The number of rats in each group for each test were shown in the Table.

Additional file 2

Figure S1. Full gels of APN, iNOS, Arg-1, NF-κB, p-NF-κB and β-actin *in vivo* and *in vitro*.

Figures

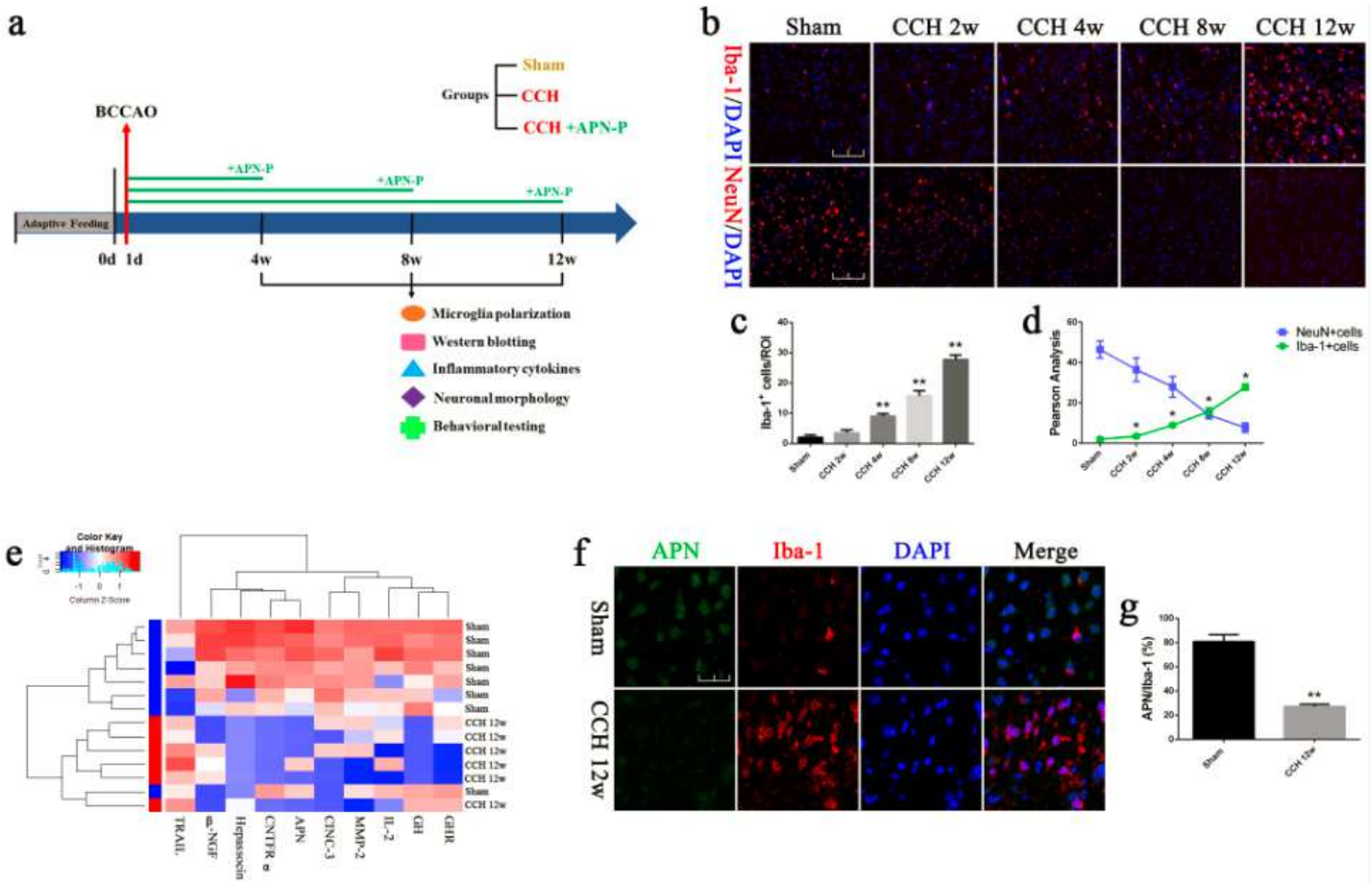

Figure 1

Microglial activation and decreased expression of APN in the cortex of CCH rats. a. A flowchart of the animal experiments. b. Representative images of Iba-1+ and NeuN+ cells in the cortexes of sham and CCH rats at the 2nd, 4th, 8th, and 12th week after BCCAO surgery. Magnification ×20, scale bar = 100 μm. c. Quantification of the Iba-1+ cells in the cortex region of rats in different groups. d. There was a negative correlation between the Iba-1+ and NeuN+ cell numbers. Values are mean ± SD, n = 3 slices from 4 animals per group, *P < 0.05, **P < 0.01 vs sham group, Student's t test and Pearson correlation analysis. ROI, 200μm2. e. A heat map representation of the protein level analysis of antibody arrays that show that APN was the most statistically significant among 10 proteins in the cortex of CCH 12w rats compared to the sham (fold change = -4.23, P < 0.05; n = 6 animals per group). f. Representative images of APN expression in Iba-1+ cells in the cortex region of sham and CCH rats at the 12th week after BCCAO surgery. Magnification ×60, scale bar = 30 μm. g. Quantification of the ratio of APN in Iba-1+ cells in cortex region. Values are mean ± SD, n = 3 slices from 3 animals per group, **P < 0.01 vs sham group, Student's t test. ROI, 100μm2.

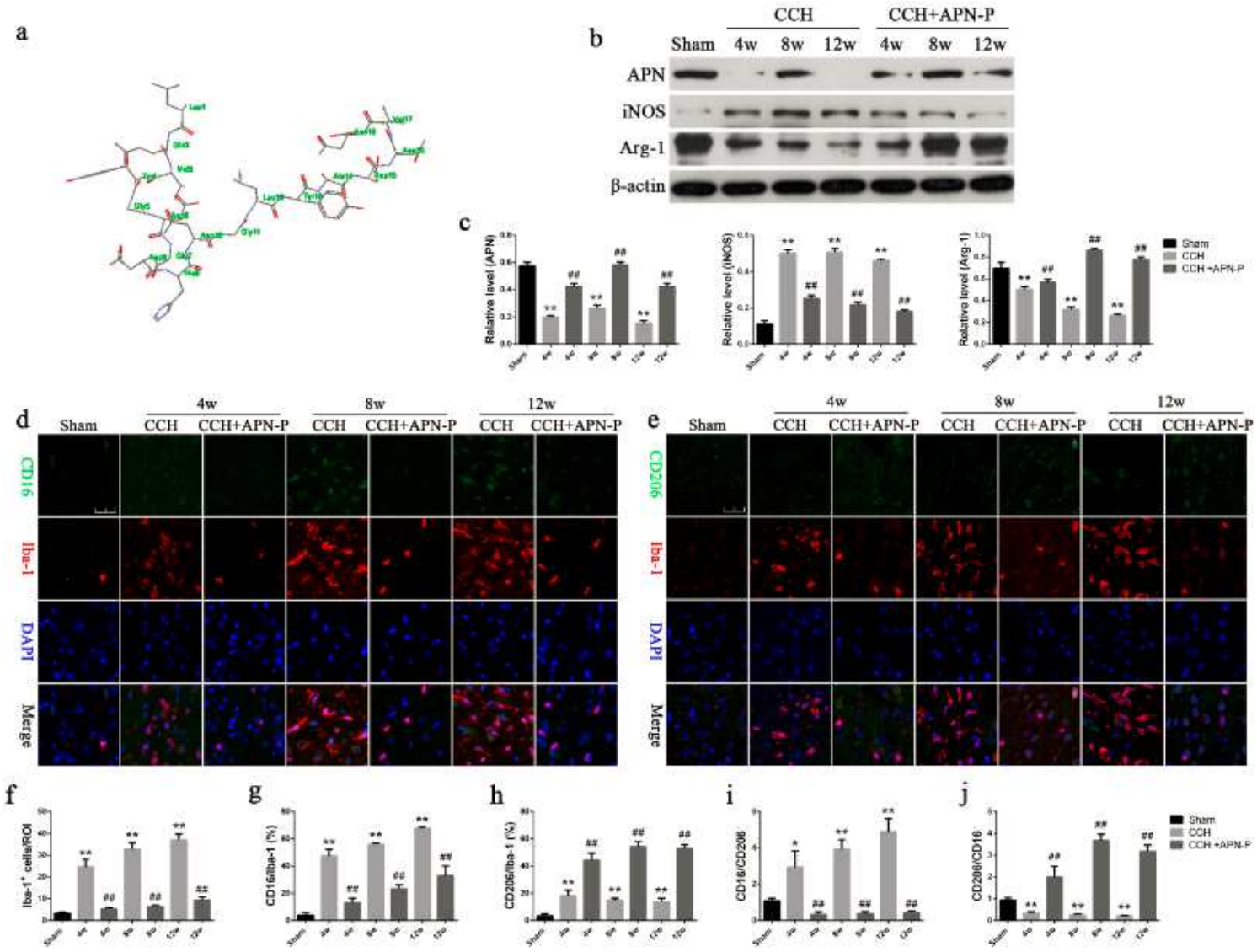

Figure 2

CCH polarizes microglia toward M1 phenotypes, while APN-P promotes M2 phenotypes in the rat cortex a. The amino acid sequence of APN-P [23]. b, c. Western blotting analysis of the relative protein levels of APN, iNOS, and Arg-1 expressed in vivo. d. Representative images of CD16 expression in Iba-1+ cells in the cortex of sham, CCH, and CCH rats with APN-P treatment groups. Magnification ×60, scale bar = 30 μm. e. Representative images of CD206 expression in Iba-1+ cells in cortex of sham, CCH and, CCH with APN-P treatment groups. Magnification ×60, scale bar = 30 μm. f. Quantification of the Iba-1+ cell number in the cortex of different treatment groups. g. Quantification of CD16 in Iba-1+ cells (%) in the cortex of different treatment groups. h. Quantification of CD206 in Iba-1+ cells (%) in the cortex of different groups. i. Quantification of the CD16/CD206 ratio in the cortex of different treatment groups. j. Quantification of the CD206/CD16 ratio in the cortex of different treatment groups. Values are mean ± SD, n = 3 slices from 3 animals per group, **P < 0.01 CCH vs sham groups, ##P < 0.01 CCH+APN-P vs CCH groups, One way ANOVA test, Tukey tests. ROI, 100μm2.

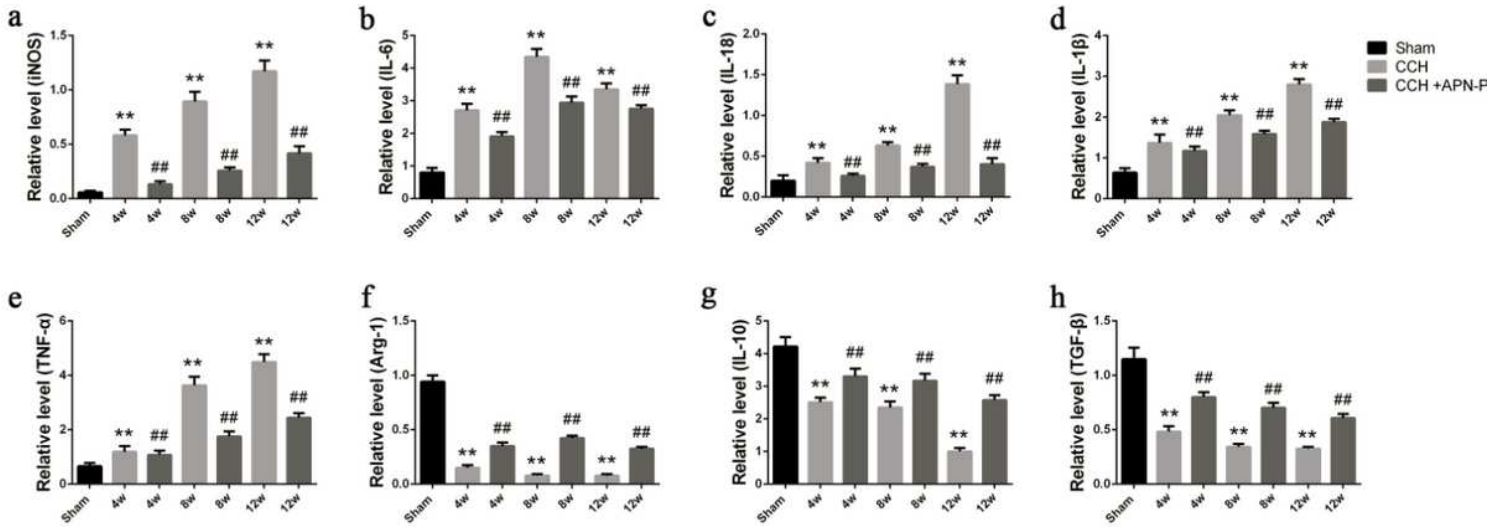

Figure 3

CCH induces inflammatory responses, while APN-P treatment induces anti-inflammatory responses in the rat cortex the mRNA expression of (a) iNOS, (b) IL-6, (c) IL-18, (d) IL-1β, (e) TNF-α, (f) Arg-1, (g) IL-10, and (h) TGF-β in the cortex of rats in different groups. Values are mean ± SD, n = 6 animals per group, **P < 0.01 CCH vs sham groups, ##P < 0.01 CCH+APN-P vs CCH groups, One way ANOVA test, Tukey tests.

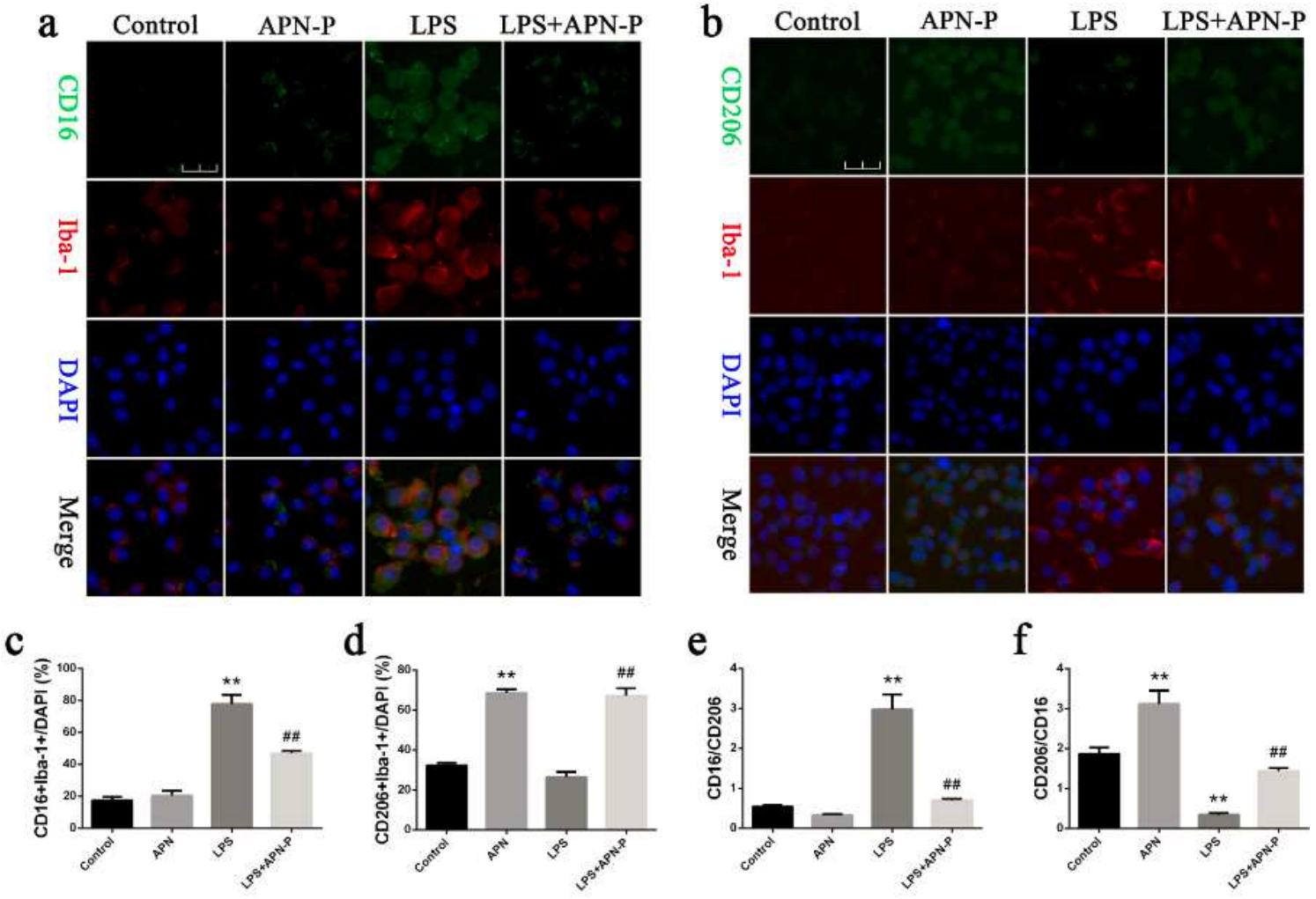

Figure 4

APN-P promotes the microglia M2 phenotype in LPS-induced BV2 cells Representative immunofluorescent images of (a) CD16 and (b) CD206 expression in Iba-1+ cells in BV2 cells from control, LPS, and LPS+APN-P treatment groups. Magnification ×60, scale bar = 30 μm. Quantification of (c) CD16 in Iba-1+ cells (%), (d) CD206 in Iba-1+ cells (%), (e) CD16/CD206 ratio, and (f) CD206/CD16 ratio in BV2 cells of different groups. Values are mean ± SD, n = 3 slices from 3 animals per group, **P < 0.01 LPS vs control group, ##P < 0.01 vs LPS group, One way ANOVA test, Tukey tests. ROI, 100μm2.

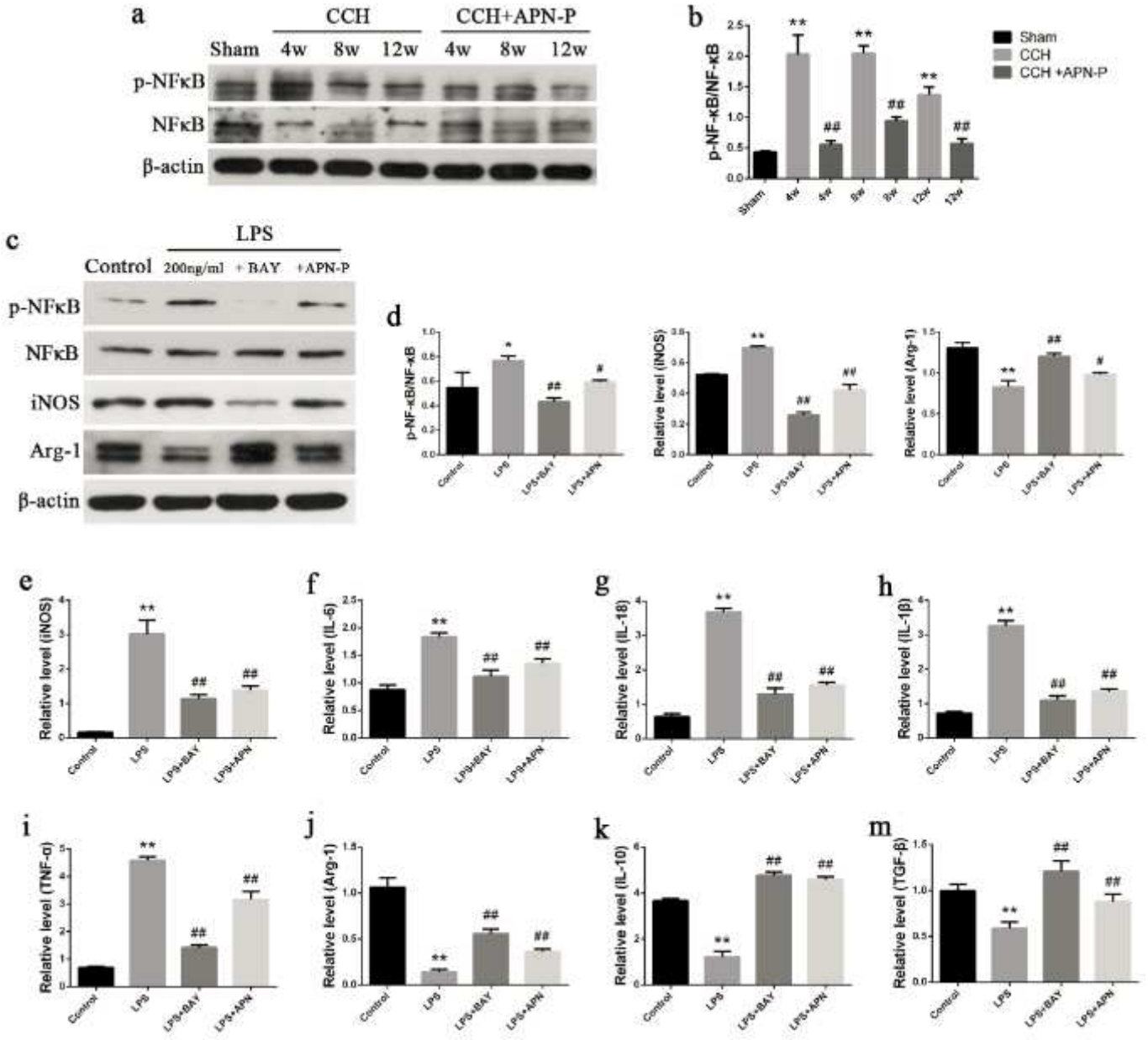

Figure 5

APN-P promotes the microglial M2 phenotype and anti-inflammatory responses via NF-κB pathway inhibition a. Western blotting analysis of in vivo NF-κB and p-NF-κB protein expression. b. Quantification of the in vivo p-NF-κB/NF-κB ratio. Values are mean ± SD, n = 3 samples per group, **P0.01 CCH vs sham group, ##P0.01 CCH+APN-P vs CCH group, One way ANOVA test, Tukey tests. c. Western blotting

analysis of the protein expression of NF-κB, p-NF-κB, iNOS and Arg-1 in vivo. d. Quantification of the in vitro p-NF-κB/NF-κB ratio relative to iNOS and Arg-1 expression levels in control, LPS treatment, LPS + BAY and LPS + APN-P treated groups. Values are mean ± SD, n = 3 samples per group, *P < 0.05, **P 0.01 LPS vs control group, #P < 0.05, ##P0.01 vs LPS group, One way ANOVA test, Tukey tests. The mRNA expression of (e) iNOS, (f) IL-6, (g) IL-18, (h) IL-1β, (i) TNF-α, (j) Arg-1, (k) IL-10, and (m) TGF-β in BV2 cells in different groups. Values are mean ± SD, n = 6 samples per group, **P0.01 LPS vs control group, ##P0.01 vs LPS group, One way ANOVA test, Tukey tests.

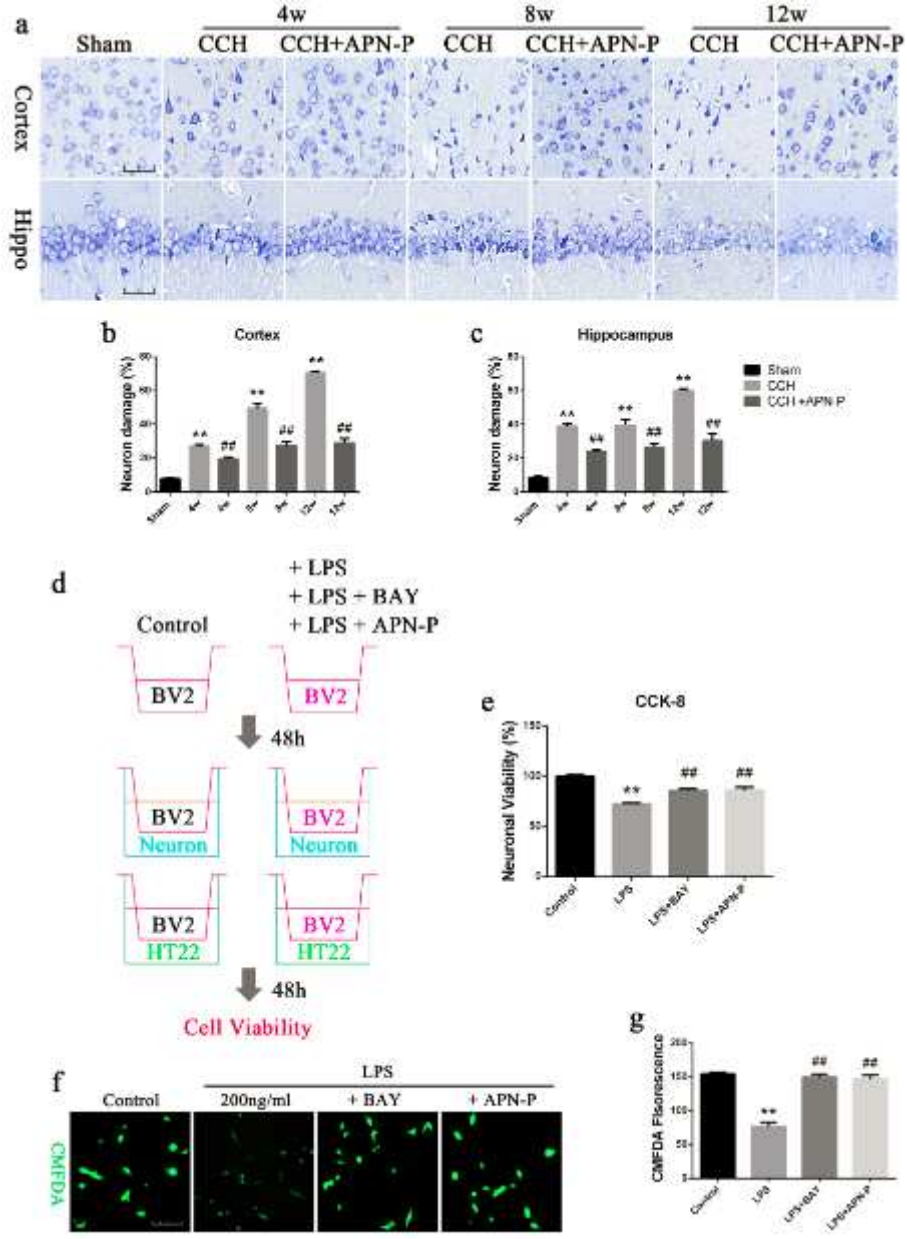

Figure 6

Effects of APN-P on neuron protection a. Sections of the cortex and the hippocampal CA1 region were obtained and treated with Nissl staining. Magnification ×40, scale bar = 50 μm. b. Quantitative analysis of neuronal damage of the cortex region. c. Quantitative analysis of neuronal damage of the hippocampal CA1 region. Values are mean ± SD, n = 3 samples per group, **P0.01 CCH vs sham group,

##P0.01 CCH+APN-P vs CCH group, One way ANOVA test, Tukey tests. ROI, 200μm2. d. Flowchart of in vitro experiments (a microglia-neuron co-culture system). e. Quantitative analysis of neuronal viability of BV2 cells from different groups after co-culturing using a CCK-8 test. Values are mean ± SD, n = 5 samples per group, **P0.01 LPS vs control group, ##P0.01 vs LPS group, One way ANOVA test, Tukey tests. f. Representative images of CMFDA-labeled neurons (green) after co-culturing with different BV2 cells. Magnification ×40, scale bar = 100 μm. g. The quantification of the CMFDA fluorescence intensity in different groups. Values are mean ± SD, n = 3 samples per group, **P0.01 LPS vs control group, ##P 0.01 vs LPS group, One way ANOVA test, Tukey tests.

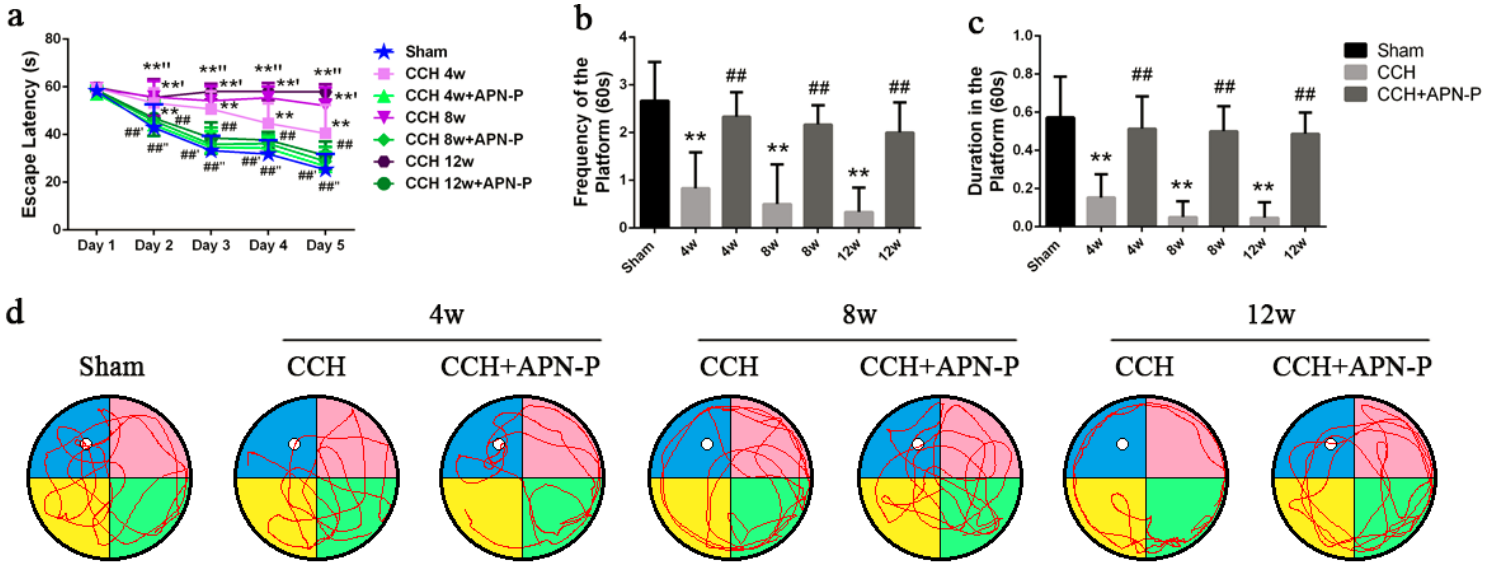

Figure 7

CCH exacerbates cognitive deficits, while APN-P improved cognitive function in rats a. EL of rats trained in a Morris water maze (day 1 to day 5). Values are mean ± SD, n = 6 samples per group, **P < 0.01 CCH 4w vs sham group, ##P < 0.01CCH 4w + APN-P vs CCH 4w group; **'P < 0.01 CCH 8w vs sham group, ##'P < 0.01 CCH 8w + APN-P vs CCH 8w group; **"P < 0.01 CCH 12w vs sham group, ##"P < 0.01 CCH 12w + APN- P vs CCH 12w group, Two-way ANOVA, Bonferroni post hoc test. b. Number of platform location crosses indicating that the CCH and CCH+APN-P treatment groups were significantly different from each other on day 6. c. Stay time of each treatment group on the platform during a single 60-s probe trial (day 6). Values are mean ± SD, n = 6 samples per group, **P < 0.01 CCH vs sham group, ##P < 0.01 CCH + APN-P vs CCH group, Two-way ANOVA, Bonferroni post hoc test. d. Representative images of the number of platform location crosses of each treatment group in the Morris water maze.

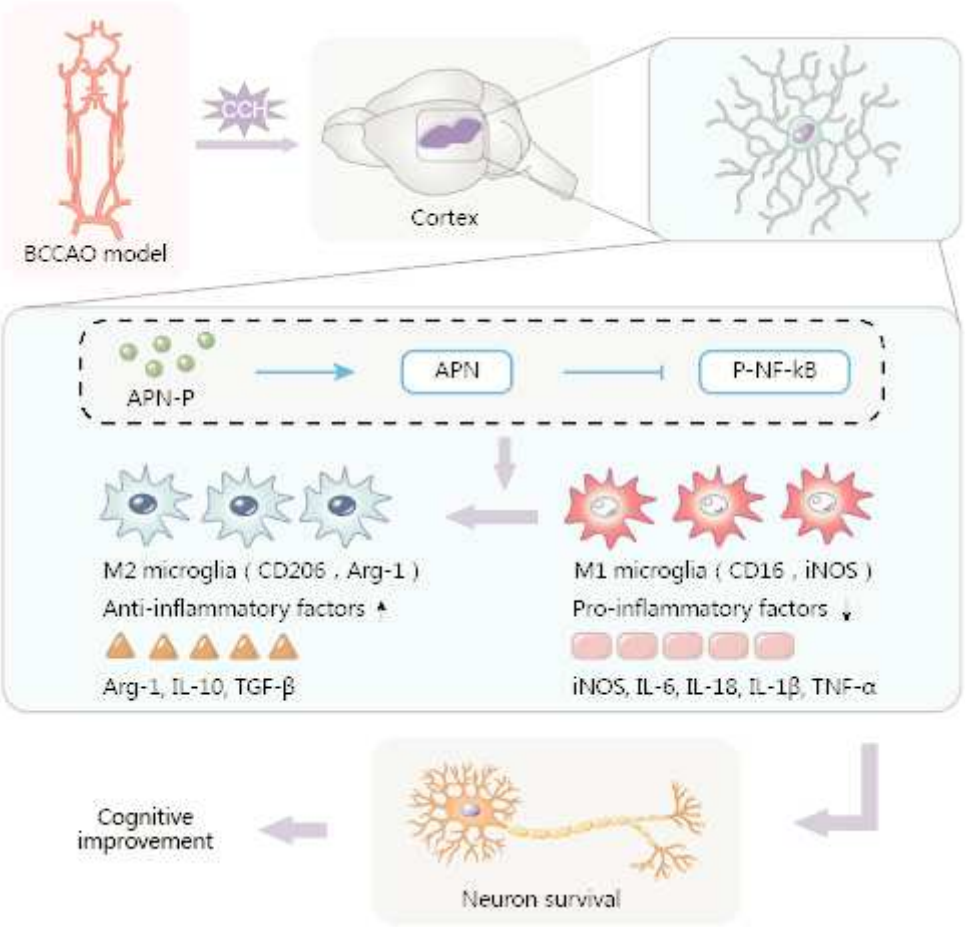

Figure 8

Graphical abstract APN-P inhibited the NF-κB pathway and regulated microglial polarization from an M1 toward an M2 phenotype, which alleviated the inflammatory response and cortical neural injury, rescuing CCH-induced cognitive impairment.

Supplementary Files

This is a list of supplementary files associated with this preprint. Click to download.

- Additionalfile1TableS1.docx
- Additionalfile2FigureS1.tif